Kinetic modeling study of benzene and PAH formation in laminar methane flames

Hanfeng Jin [a], Alessio Frassoldati [b], Yizun Wang [a], Xiaoyuan Zhang [c], Meirong Zeng [c], Yuyang Li [a], Fei Qi [a,c,*], Alberto Cuoci [b], Tiziano Faravelli [b]

[a] State Key Laboratory of Fire Science, University of Science and Technology of China, Hefei, Anhui 230026, PR China
[b] Department of Chemistry, Materials, and Chemical Engineering, Politecnico di Milano, Piazza Leonardo da Vinci 32, 20133 Milano, Italy
[c] National Synchrotron Radiation Laboratory, University of Science and Technology of China, Hefei, Anhui 230029, PR China

Received 7 September 2014
Received in revised form 25 November 2014
Accepted 25 November 2014
Available online 6 January 2015

1. Introduction

Soot is a health, environmental, and mechanical hazard, whose formation mechanism is still not completely clear up to now. Polycyclic aromatic hydrocarbons (PAHs) are recognized as the main precursors of soot particles. The control of the formation of PAHs is then a critical issue in the combustion process, which are significantly affected by the uniformity of the fuel/oxidizer mixture, the ignition method, and the fuel combustion chemistry. Fundamental knowledge of the processes leading to the aromatic growth in flames, from fuel-decomposed small species to PAH and soot, will benefit the scientific researchers and engineers in their design of fuels, engines and large power generation systems.

Methane, that is the simplest hydrocarbon molecule and the dominant component in natural gas (up to 90–95% in vol.), is the main energy supply of domestic gas appliances. Therefore, it is the most frequently investigated hydrocarbon fuel. Early studies were mainly focused on its ignition property [1–4] and burning velocity [5–8]. The oxidation of methane was investigated in flow reactor [9,10], jet-stirred reactor [11–14], and shock tube [15–17]. Kinetic studies on the chemical structures of methane flames started in 1980s [18–20]. Later, a variety of premixed methane flames were investigated experimentally [21–26]. Meanwhile, a set of experiments were also performed in non-premixed flames, in order to observe the flame structures and spatial distribution of combustion intermediates [27–31]. Oxygenates [30], small unsaturated hydrocarbons [27–31], benzene [27–31] and PAHs [27–29] were observed with gas chromatography (GC) or mass spectrometry (MS).

Today, thanks to the considerable progresses made over the last few decades, several kinetic models [32–36] can predict methane combustion properties fairly well, including the ignition delay time, the burning velocity, and the oxidation processes. However, there is still lack of knowledge on PAH formation in methane flames, which attracts even greater interests, since it reveals a

* Corresponding author at: National Synchrotron Radiation Laboratory, University of Science and Technology of China, Hefei, Anhui 230029, PR China. Fax: +86 551 65141078.
E-mail address: fqi@ustc.edu.cn (F. Qi).

complete map of the carbon chain growth and the aggregation of small molecules to aromatic species.

In early studies, Marinov et al. [26,27] extended their detection of intermediates to three-rings PAHs in their experimental investigations of premixed and counter flow diffusion flames. Meanwhile, a kinetic model was developed to describe the multi-pathways of the benzene and PAH formation. They concluded that the reaction between allyl and propargyl radicals is the primary benzene formation pathway, occurring via the isomerization of fulvene. According to their modeling study, reaction of benzyl and propargyl radicals provides a larger contribution than the self-combination of cyclopentadienyl radical to naphthalene formation.

D'Anna and Kent [37] modeled the coflow methane flames reported by Anderson et al. [31] using their previously developed kinetic model. Their detailed chemical analysis also showed that benzene formation is mostly controlled by the self-combination of propargyl radical. Key reactions similar to those in Marinov et al.'s work [27] were identified as the most important ones lead-ing to the formation of naphthalene, while D'Anna et al. also emphasized the contribution of the hydrogen-abstraction-acety-lene-addition (HACA) pathways [38,39].

Slavinskaya and Frank [40] established a model for the predictions of the formation of soot precursors in premixed methane flames. Later, they updated their PAH mechanism based on the further validations of ethane and ethylene flames [41,42]. Their main conclusion is that three PAH formation pathways show similar importance: HACA mechanism [38,39], the addition of small molecules to aromatic molecules/radicals [43,44], and the combination reactions of aromatic molecules and radicals [45,46]. According to their extensive model analysis, these reaction pathways give main contributions in PAH formation at $T > 1550$ K, while part of the reaction pathways proceeds in the reverse direction or achieving equilibrium when the flame temperature is lower than 1500 K.

Roesler et al. [29] investigated the role of methane and the synergistic effect between methane and ethylene on the growth of aromatic hydrocarbons, which was modeled by Cuoci et al. [47] in their computational fluid dynamic (CFD) simulations. Recently, Cuoci et al. [48] carried out an experimental and numerical study on methane coflow flames. In their work, both Polimi [33] and GRI Mech 3.0 [34] were used to reproduce the flame structure as well as benzene and naphthalene formation processes in coflow flames. Their main point confirmed that the odd pathways (via propargyl recombination) to benzene prevailed over the even pathways (characterized by a sequence of C2 species addition). Naphthalene formation was sensitive to the reaction of phenyl on acetylene and in less extent to the termination reaction of benzyl and propargyl radicals.

Therefore, it is clear that there are still many uncertainties in the understanding of benzene and PAH formation kinetics in the combustion of methane, since the quantities of benzene and PAH precursors are significantly impacted by the accuracies of the rate constants of the recombination reactions involving small molecules. There are no comprehensive kinetic modeling investigations on laminar methane flames, including the validations under the premixed, counter flow and coflow diffusion flame conditions. Based on the recent progress in the combustion kinetics of methane [36], and the efforts on the combustion of benzene [49–52], toluene [43,53–55] and naphthalene [44,46,56–59], a detailed kinetic model was developed for the combustion and PAH formation in laminar methane flames. This model was validated against the experimental data of laminar flames in various previous investigations, including the premixed flames [22–24], and the counter flow flames [60], whose operative conditions are reported in Table 1. Four different coflow methane flames (named *CF1*, *CF2*, *CF3* and *CF4*) with various nitrogen dilution ratios were diagnosed with synchrotron vacuum ultra-violate photoionization mass spectrometry (SVUV-PIMS). The experimental conditions for these coflow diffusion flames are also listed in Table 1. The methane oxidation model is also validated in respect to these experimental data. Part of the experimental data of *CF1* was reported in previous modeling study of Cuoci et al. [48]. A continuous modeling work allows improving the mechanism as presented in this work. The developed kinetic model permits an accurate prediction of the combustion intermediates, reducing for example the over prediction of the benzene precursor and aromatic species in the previous investigation of Cuoci et al. [48]. Combined with the validations in premixed and counter flow flames, this work aims at further investigating the kinetics of methane combustion in different flame conditions, especially focusing on the formation of benzene and PAHs. The discrepancies between predictions and measured values are discussed to highlight the effects of the stoichiometric ratio, mass diffusion, the dilution with inert gas and the formation of small

Table 1
Experimental conditions of laminar methane flames.

Name	P[a]	$\dot{m}$[b]	Φ	X_{Ar}	X_{O2}	X_{CH4}	Ref
Premixed flames							
PF1	6.70	0.005578	1.00	0.7020	0.1989	0.0991	[22]
PF2	101.3	0.006180	2.60	0.4530	0.2378	0.3092	[24]
PF3	101.3	0.007019	2.60	0.4500	0.2391	0.3109	[23]

Name	P[a]	$T_{oxidizer}$[c]	T_{fuel}[c]	$v_{oxidizer}$[d]	v_{fuel}[d]	Oxidizer		Fuel		Ref
						X_{N2}	X_{O2}	X_{CH4}	X_{N2}	
Counter flow diffusion flames										
OF1	101.3	300	300	70.00	70.00	0.79	0.21	1.00	0.00	[60]

Name	P[a]	Q_{air}[e]	Q_{Ar}[e]	Q_{N2}[e]	Q_{CH4}[e]	v_{air}[d]	v_{fuel}[d]
Coflow diffusion flames							
CF1	101.3	160,000	5.87	314	308	36.21	14.64
CF2	101.3	160,000	5.87	345	277	36.21	14.64
CF3	101.3	160,000	5.87	377	245	36.21	14.64
CF4	101.3	160,000	5.87	408	214	36.21	14.64

[a] P, environment pressure, Unit: kPa.
[b] $\dot{m}$, mass flow rate, Unit: g/(s cm^2).
[c] T, temperature of fuel/oxidizer stream, Unit: K.
[d] v_i, mean velocity of fuel/oxidizer stream, Unit: cm/s.
[e] Q_i, flow rate of species i, Unit: SCCM.

molecules. Key reactions in the combustion of methane and the main pathways leading to PAHs were identified for the different flame conditions.

2. Experimental methods

Methane coflow diffusion flames were diagnosed with SVUV-PIMS at National Synchrotron Radiation Laboratory in Hefei, China. The experimental apparatus for the investigation of laminar coflow diffusion flame used in this work was discussed in detail in previous studies [48,61], including a laminar coflow flame burner, a probe sampling system, a time-of-flight mass spectrometer and a synchrotron-based photoionization source. The coflow flames were generated at atmospheric pressure by a burner with a 10-mm-ID (inner diameter) fuel tube located in the center of a 102-mm-ID air tube. Four flames were investigated in this work varied by dilu-tion ratio of nitrogen in the fuel mixture. The flow rates of fuels (CH_4), diluent gas (N_2), calibration gas (Ar) and air are presented in Table 1. The purities of CH_4, N_2, O_2, and Ar are 99.995%, 99.999%, 99.999%, and 99.99%, respectively. The mean velocities of fuel mixture and air were 14.64 and 36.21 cm/s at 300 K in all four flames, respectively. The gas flow rates were regulated by mass flow controllers.

Flame species along the flame centerline were sampled for the successive calculation of their mole fraction profiles. The detailed flame sampling and data evaluation procedures were introduced in detail in [61]. Mole fraction values cannot be measured in the region close to the nozzles, due to the shape limit of the sampling probe. The uncertainty of the experimental measurements is related to the probe sampling process and the photoionization cross sections (PICS, available in the database of [62]) of flame species. The uncertainties of the measured mole fractions are within ±20% for flame species calculated with cold gas calibration, ±50%for stable flame species with well-known PICSs, and about a factor of 2 for free radicals and the flame species with estimated PICSs [48,61]. Flame temperature profiles along the flame centerline were measured by Pt–6%Rh/Pt–30%Rh thermocouples, 0.1 mm in diameter, coated with Y_2O_3–BeO anti-catalytic ceramic to avoid catalytic effects [63]. The soot deposition effect on the thermocouples was partially corrected in the post-calibration of radiative heat loss. The uncertainty of the temperature measurement is about± 50 K. And the gas temperature at the sooting area in the flame could be underestimated by about 120 K. All the experimental data as well as the PICSs of flame species are provided in the Supple-mentary Material, convenient for other modeling validations.

3. Kinetic model construction

The methane mechanism in this work was based on USC Mech II with deep development and extension. This mechanism consists of 213 species and 1466 reactions, provided in the Supplementary Material in CHEMKIN format, whilst the main reactions are reported in Table 2. As mentioned, this mechanism was validated in previous investigations of laminar flames [50,53,61,64,65]. The aromatic formation submechanism was improved based on our previous investigations [53,56,66], recent theoretical calculations [43,44,51,67] and other aromatic mechanisms [54,57,68–70], mainly including HACA (hydrogen-abstraction acetylene-addition) pathways [39] and the recombination reactions of resonantly stabilized radicals with small flame species [37,53,68–70].

3.1. Submechanism of methane

Unimolecular decomposition of methane (R1) is a sensitive reaction for the prediction of ignition delay time [2] and laminar flame speed [8] of methane. The rate constant of (R1) was adopted from GRI Mech 2.11 [71]. The same value was adopted in USC Mech II [35], Polimi Mech [33] and Aramco Mech 1.0 [36]. A higher rate was recommended in GRI Mech 3.0 [34] and in the calculation of Klippenstein and co-workers [72], because of the higher high-pressure limits. (R2), (R3), (R4) are H-abstraction reactions of methane by H, OH and O radicals. The rate constant of (R2) was adopted from the review of Baulch et al. [73] recommended in Aramco Mech 1.0 [36]. It is very similar to the values used in GRI Mech 3.0 [34] and Polimi Mech [33]. Metcalfe et al. [36] evaluated a set of rate constant value for (R3) by fitting NIST data. Meanwhile, Srinivasan et al. [74] measured this reaction in shock tube experi-ment. In the model of this work, (R3) and (R4) were referred to GRI Mech 3.0 [34].

$$CH_3 + H(+M) = CH_4(+M) \quad (R1)$$

$$CH_4 + H = CH_3 + H_2 \quad (R2)$$

$$CH_4 + OH = CH_3 + H_2O \quad (R3)$$

$$CH_4 + O = CH_3 + OH \quad (R4)$$

The major oxidation pathways of methyl radical are the reactions with O, OH and O_2. Reaction between methyl radical and O atom (R5) and (R6) was theoretically investigated in the work of Harding et al. [75]. A competitive additional channel (R6) was suggested with a branching ratio of 0.18, while only (R5) was considered in USC Mech II [35] and GRI Mech 3.0 [34]. Compared to the rate constant of (R5) recommended in these two mechanisms, 8.43×10^{13} and 5.06×10^{13}, respectively, the value adopted in this model is slightly smaller. (R7), (R8), (R9), (R10), (R11) are the most important channels for the reactions of methyl and hydroxyl radicals. They were upgraded with the theoretical calculations of Jasper et al. [76], which were also recommended in the work of Sarathy et al. [77] and Metcalfe et al. [36]. Two channels of the reaction between methyl radical and oxygen molecule (R12) and (R13) were considered, which produce CH_3O radical and formaldehyde, respectively. The rate constants of (R12) was adopted from the work of Srinivasan et al. [78] and (R13) was adopted from the recommendation of Aul et al. [2]. The rate constants of (R12) is very close to the values of other mechanisms [33–35], while the value of (R13) shows a significant difference in the low temper-ature region. CH_3 + HO_2 reactions (R14 and R15, listed in Table 2) are important in the low temperature oxidation of methane, how-ever, they are not sensitive in the flames investigated in this work.

$$CH_3 + O = CH_2O + H \quad (R5)$$

$$CH_3 + O = HCO + H_2 \quad (R6)$$

$$CH_3 + OH(+M) = CH_2O + H_2(+M) \quad (R7)$$

$$CH_3OH(+M) = CH_3 + OH(+M) \quad (R8)$$

$$CH_3 + OH = CH_2^* + H_2O \quad (R9)$$

$$CH_3 + OH = CH_3O + H \quad (R10)$$

$$CH_3 + OH = CH_2OH + H \quad (R11)$$

$$CH_3 + O_2 = O + CH_3O \quad (R12)$$

$$CH_3 + O_2 = OH + CH_2O \quad (R13)$$

Self-combination of methyl radical (R16) is a very sensitive reaction to the carbon chain growth in methane flames. The rate constant used in this model was taken from the expression in

Table 2
Selected reactions in the present kinetic model.[a]

No.	Reactions	A	*n*	Ea	Reference
R1	$CH_3 + H (+M) = CH_4 (+M)$	1.27×1016	−0.63	383.0	[71]
	Low	2.48×10^{33}	−4.76	2440.0	
	Troe	0.783 74.0 2941.0 6964.0			
	H_2/2.0/H_2O/6.0/CH_4/2.0/CO/1.5/CO_2/2.0/C_2H_6/3.0/AR/0.7/				
R2	$CH_4 + H = CH_3 + H_2$	6.14×10^5	2.50	9587.0	[73]
R3	$CH_4 + OH = CH_3 + H_2O$	1.00×10^8	1.60	3120.0	[34]
R4	$CH_4 + O = CH_3 + OH$	1.02×10^9	1.50	8600.0	[34]
R5	$CH_3 + O = CH_2O + H$	4.54×10^{13}	0.05	−136.0	[75]
R6	$CH_3 + O = HCO + H_2$	9.97×10^{12}	0.05	−136.0	[75]
R7	$CH_3 + OH (+M) = CH_2O + H_2 (+M)$	5.88×10^{-14}	6.72	−3022.2	[76]
	Low	2.82×10^5	1.47	−3270.6	
	Troe	1.671 434.8 2934.2 3919.0			
R8	$CH_3OH (+M) = CH_3 + OH (+M)$	2.08×10^{18}	−0.62	92540.6	[76]
	Low	1.50×10^{43}	−7.00	97992.2	
	Troe	−0.475 35,580 1116.0 9023.0			
R9	$CH_3 + OH = CH_2^* + H_2O$				[76]
	Plog 0.01	4.94×10^{14}	−0.67	−445.8	
	Plog 0.10	1.21×10^{15}	−0.78	−175.6	
	Plog 1.00	5.28×10^{17}	−1.52	1772.0	
	Plog 10.0	4.79×10^{23}	−3.16	7003.0	
	Plog 100.	8.43×10^{19}	−1.96	8244.0	
R10	$CH_3 + OH = CH_3O + H$				[76]
	Plog 0.01	1.19×10^9	1.02	11940.0	
	Plog 0.10	1.19×10^9	1.02	11940.0	
	Plog 1.00	1.23×10^9	1.01	11950.0	
	Plog 10.0	1.80×10^9	0.97	12060.0	
	Plog 100.	5.24×10^{10}	0.55	13070.0	
R11	$CH_3 + OH = CH_2OH + H$				[76]
	Plog 0.01	1.62×10^{10}	0.97	3214.0	
	Plog 0.10	1.81×10^{10}	0.95	3247.0	
	Plog 1.00	4.69×10^{10}	0.83	3566.0	
	Plog 10.0	1.53×10^{13}	0.13	5641.0	
	Plog 100.	3.59×10^{14}	−0.19	8601.0	
R12	$CH_3 + O_2 = O + CH_3O$	7.55×10^{12}	0.00	28320.0	[78]
R13	$CH_3 + O_2 = OH + CH_2O$	2.61	3.28	8105.0	[2]
R14	$CH_3 + HO_2 = CH_4 + O_2$	1.16×10^5	2.23	−3022.0	[136]
R15	$CH_3 + HO_2 = CH_3O + OH$	1.00×10^{12}	0.27	−687.5	[136]
R16	$CH_3 + CH_3 (+M) = C_2H_6 (+M)$	2.12×10^{16}	−0.97	620.0	[71]
	Low	1.77×10^{50}	−9.67	6220.0	
	Troe	0.533 151.0 1038.0 4970.0			
	H_2/2.0/H_2O/6.0/CH_4/2.0/CO/1.5/CO_2/2.0/C_2H_6/3.0/AR/0.7/				
R17	$CH_3 + CH_3 = H + C_2H_5$	3.01×10^{13}	0.00	13513.4	[83]
R18	$H + C_2H_4 (+M) = C_2H_5 (+M)$	9.57×10^8	1.46	1355.0	[2]
	Low	1.42×10^{39}	−6.64	5769.0	
	Troe	−0.569 299.0 −9147 152.4			
	H_2/2.0/H_2O/6.0/CH_4/2.0/CO/1.5/CO_2/2.0/C_2H_6/3.0/AR/0.7/				
R19	$C_2H_5 + H = C_2H_4 + H_2$	4.21×10^{12}	0.00	0.0	[73]
R20	$C_2H_5 + O = CH_3CHO + H$	2.90×10^{12}	0.03	−394.0	[75]
R21	$C_2H_5 + O = CH_3 + CH_2O$	1.88×10^{13}	0.03	−394.0	[75]
R22	$C_2H_5 + O = C_2H_4 + OH$	3.80×10^{12}	0.03	−394.0	[75]
R23	$C_2H_5 + O_2 = C_2H_4 + HO_2$ Duplicate				[137]
	Plog 0.04	2.09×10^9	0.49	−391.4	
	Plog 1.00	1.84×10^7	1.13	−720.6	
	Plog 10.0	7.56×10^{14}	−1.01	4749.0	
	$C_2H_5 + O_2 = C_2H_4 + HO_2$ Duplicate	6.61	3.51	14160.0	
R24	$C_2H_5 + O_2 = CH_3CHO + OH$				[137]
	Plog 0.04	4.91×10^{-6}	4.76	254.3	
	Plog 1.00	6.80×10^{-2}	3.57	264.3	
	Plog 10.0	8.27×10^2	2.41	5285.0	
R25	$C_2H_4 + H = C_2H_3 + H_2$	5.07×10^7	1.90	12950.0	[35]
R26	$C_2H_4 + OH = C_2H_3 + H_2O$	3.60×10^6	2.00	2500.0	[35]
R27	$C_2H_4 + CH_3 = C_2H_3 + CH_4$	6.62	3.70	9500.0	[95]
R28	$C_2H_3 (+M) = C_2H_2 + H (+M)$	3.86×10^8	1.62	37048.2	[35]
	Low	2.56×10^{27}	−3.40	35798.7	
	Troe	1.982 5383.7 4.2932 −0.0795			
	H_2/2.0/H_2O/6.0/CH_4/2.0/CO/1.5/CO_2/2.0/C_2H_6/3.0/AR/0.7/C_2H_2/3.0				
R29	$C_2H_4 (+M) = H_2 + H_2CC (+M)$	8.00×10^{12}	0.44	88770.0	[35]
	Low	7.00×10^{50}	−9.31	99860.0	
	Troe	0.7345 180.0 1035.0 5417.0			
	H_2/2.0/H_2O/6.0/CH_4/2.0/CO/1.5/CO_2/2.0/C_2H_6/3.0/AR/0.7/				
R30	$C_2H_2 (+M) = H_2CC (+M)$	8.00×10^{14}	−0.52	50750.0	[35]
	Low	2.45×10^{15}	−0.64	49700.0	
	H_2/2.0/H_2O/6.0/CH_4/2.0/CO/1.5/CO_2/2.0/C_2H_6/3.0/C_2H_2/2.5/C_2H_4/2.5/				

(*continued on next page*)

Table 2 (*continued*)

No.	Reactions	A	*n*	Ea	Reference
R31	$C_2H_5 + CH_3$ (+M) = C_3H_8 (+M)	7.35×10^{14}	−0.50	0.0	[95]
	Low	1.02×10^{62}	−13.42	6000.0	
	Troe	1.000 1000.0 1433.9 5328.8			
	H_2/2.0/H_2O/6.0/CH_4/2.0/CO/1.5/CO_2/2.0/C_2H_6/3.0/AR/0.7/				
R32	$C_2H_3 + CH_3$ (+M) = C_3H_6 (+M)	2.50×10^{13}	0.00	0.0	[35]
	Low	4.27×10^{58}	−11.94	9769.8	
	Troe	0.175 1340.6 60,000 10139.8			
	H_2/2/H_2O/6/CH_4/2/CO/1.5/CO_2/2/C_2H_6/3/AR/0.7/C_2H_2/3/C_2H_4/3/				
R33	$C_3H_6 + H = C_2H_4 + CH_3$				[138]
	Plog 0.10	8.80×10^{16}	−1.05	6461.0	
	Plog 1.00	8.00×10^{21}	−2.39	11180.0	
	Plog 10.0	3.30×10^{24}	−3.04	15610.0	
R34	$C_2H_2 + CH_3 = pC_3H_4 + H$				[97]
	Plog 0.10	4.50×10^{6}	1.86	11600.0	
	Plog 1.00	2.56×10^{9}	1.10	13644.0	
	Plog 2.00	2.07×10^{10}	0.85	14415.0	
	Plog 5.00	2.51×10^{11}	0.56	15453.0	
	Plog 10.0	1.10×10^{12}	0.39	16200.0	
	Plog 100.	2.10×10^{12}	0.37	18100.0	
R35	$C_2H_2 + CH_3 = aC_3H_4 + H$				[97]
	Plog 0.10	2.40×10^{9}	0.91	20700.0	
	Plog 1.00	5.14×10^{9}	0.86	22153.0	
	Plog 2.00	1.33×10^{10}	0.75	22811.0	
	Plog 5.00	9.20×10^{10}	0.54	23950.0	
	Plog 10.0	5.10×10^{11}	0.35	25000.0	
	Plog 100.	7.30×10^{12}	0.11	28500.0	
R36	$C_3H_3 + C_3H_3 = A_1$				[98]
	Plog 1.00	1.07×10^{45}	−9.57	17015.0	
	Plog 10.0	7.17×10^{40}	−8.24	15920.0	
R37	$pC_3H_4 + C_3H_3 = A_1 + H$	2.20×10^{11}	0.00	2000.0	[37]
R38	$aC_3H_4 + C_3H_3 = A_1 + H$	2.20×10^{11}	0.00	2000.0	[37]
R39	Fulvene = A_1				[99]
	Plog 0.04	5.62×10^{81}	−19.36	121500.0	
	Plog 1.00	1.45×10^{45}	−8.90	96999.0	
	Plog 10.0	2.95×10^{31}	−4.97	88465.0	
R40	Fulvene + H = A_1 + H				[51]
	Plog 0.013	2.15×10^{22}	−2.28	8429.0	
	Plog 0.132	5.60×10^{26}	−3.47	12818.0	
	Plog 1.000	1.66×10^{25}	−2.99	13691.0	
	Plog 1.312	5.06×10^{25}	−3.12	14226.0	
	Plog 13.12	2.20×10^{27}	−3.48	19199.0	
R41	$C_3H_3 + aC_3H_5$ = Fulvene + 2H	3.26×10^{29}	−5.40	3390.0	[105]
R42	$C_3H_3 + C_3H_3 = A_1$- + H				[98]
	Plog 1.00	5.77×10^{37}	−7.00	31506.0	
	Plog 10.0	3.87×10^{33}	−5.67	30411.0	
R43	$C_3H_2 + C_3H_3 = A_1$-	7.00×10^{12}	0.00	0.0	[107]
R44	A_1CH_3 (+M) = A_1- + CH_3 (+M)	1.95×10^{27}	−3.16	107447.0	[109]
	Low	1.00×10^{98}	−22.97	122080.0	
	Troe	0.705 1×10^{10} 459.9 8.21×10^{9}			
R45	$A_1CH_3 + H = A_1 + CH_3$	5.78×10^{13}	0.00	8095.0	[139]
R46	A_1CH_3 (+M) = A_1CH_2 + H (+M)	2.78×10^{15}	0.17	91168.0	[109]
	Low	1.00×10^{98}	−22.86	99882.0	
	Troe	0.0655 15.11 1×10^{9} 7.60×10^{7}			
R47	$A_1CH_3 + H = A_1CH_2 + H_2$	6.47	3.98	3394.0	[111]
R48	$A_1CH_3 + OH = A_1CH_2 + H_2O$	1.77×10^{5}	2.39	−602.0	[112]
R49	$A_1CH_2 + H = A_1$- + CH_3				[109]
	Plog 0.04	4.50×10^{58}	−11.90	51860.0	
	Plog 0.13	2.03×10^{64}	−13.37	59520.0	
	Plog 1.00	5.83×10^{67}	−14.15	68330.0	
	Plog 10.0	8.85×10^{68}	−14.23	78410.0	
R50	A_1- + $C_3H_3 = C_9H_8$	1.00×10^{13}	0.00	0.0	[113]
R51	$A_1 + C_3H_3 = C_9H_8 + H$	6.26×10^{9}	2.61	56500.0	[54]
R52	$A_1CH_2 + C_2H_2 = C_9H_8 + H$	3.16×10^{4}	2.50	11061.2	[69]
R53	$A_1CH_2 + C_3H_3 = C_9H_7CH_2 + H$	5.00×10^{13}	0.00	8000.0	This work
R54	$C_9H_7CH_2 = C_9H_6CH_2 + H$				[44]
	Plog 0.0013	6.28×10^{71}	−18.20	65710.8	
	Plog 0.0132	2.82×10^{61}	−14.81	62789.9	
	Plog 0.1316	3.77×10^{47}	−10.44	58071.8	
	Plog 1.00	7.54×10^{33}	−6.23	52769.3	
	Plog 10.0	4.44×10^{21}	−2.49	47796.0	
	Plog 100.	2.86×10^{13}	0.02	44394.9	
R55	$C_9H_7CH_2 = A_2 + H$				[44]
	Plog 0.0013	3.68×10^{63}	−15.81	57409.9	
	Plog 0.0132	6.88×10^{51}	−12.10	53279.3	
	Plog 0.1316	2.37×10^{38}	−7.92	48317.2	

Table 2 (*continued*)

No.	Reactions	A	*n*	Ea	Reference
	Plog 1.00	9.04×10^{25}	−4.12	43307.9	
	Plog 10.0	4.13×10^{16}	−1.28	39451.4	
	Plog 100.	5.55×10^{12}	−0.07	38027.7	
R56	$C_9H_6CH_2 + H = A_2 + H$	5.35×10^{11}	0.63	2422.4	[44]
R57	$C_9H_6CH_2 = A_2$	1.45×10^{45}	−8.90	96999.0	This work
R58	$C_7H_5 + C_3H_3 = A_2$				This work
	Plog 0.04	1.82×10^{74}	−18.14	31896.0	
	Plog 1.00	3.16×10^{55}	−12.55	22264.0	
	Plog 10.0	3.89×10^{50}	−11.01	20320.0	
R59	$C_7H_5 + C_3H_3 = A_2\text{-} + H$	1.70×10^{48}	−9.98	36755.0	This work
R60	$A_1\text{-} + C_4H_4 = A_2 + H$	1.26×10^{04}	2.61	1434.0	[69]
R61	$A_1\text{-} + nC_4H_3 = A_2$	7.51×10^{75}	−17.90	39600.0	[118]
R62	$A_1 + nC_4H_3 = A_2 + H$	4.00×10^{13}	0.00	15976.0	[53]
R63	$C_5H_5 + C_5H_5 = A_2 + 2H$	0.50×10^{13}	0.00	8000.0	[118]
R64	$A_1CHCH + C_2H_2 = A_2 + H$	1.60×10^{16}	−1.33	5400.0	[39]
R65	$A1CCH_2 + C_2H_2 = A_2 + H$	3.02×10^{3}	2.55	3181.2	[69]
R66	$A1C_2H + C_2H_3 = A_2 + H$	4.30×10^{17}	−1.33	4888.3	This work
R67	$C_9H_7 + C_3H_3 = A_2R_5 + 2H$	8.10×10^{42}	−9.20	15153.0	This work
R68	$A_2\text{-} + C_2H_2 = A_2R_5 + H$	8.20×10^{30}	−5.40	16900.0	[39]
R69	$C_9H_7 + C_4H_4 = C_{13}H_{10} + H$	3.00×10^{11}	0.00	0.0	[53,66]
R70	$A_1\text{-} + A_1\text{-} = P_2$	2.00×10^{19}	−2.05	2900.0	[39]
R71	$A_1 + A_1\text{-} = P_2 + H$	1.10×10^{23}	−2.92	15890.0	[39]
R72	$C_9H_7 + C_5H_5 = A_3 + H_2$	1.00×10^{12}	0.00	6000.0	[67]
R73	$A_2\text{-} + C_4H_4 = A_3 + H$	3.30×10^{33}	−5.70	25500.0	[39]

[a] Units: s^{-1}, cm^3, and cal/mol.

GRI Mech 2.11 [71]. The high-pressure limit provided in this work agrees well with the experimental and theoretical study of Wang et al. [79]. It is slightly lower than the value proposed by Klippenstein et al. [80], which predicted the high-pressure limits for a series of alkyl radical combination reactions. The rate constant expressions of (R16) reported by Kiefer et al. [81] and Oehlschlaeger et al. [82] were different from the studies above in the temperature dependencies. Therefore, they were not adopted in this model. As a competing channel of (R16), H and ethyl radicals are formed in (R17). The reaction expressions of (R17) were adopted from the work of Baulch et al. [83].

$$CH_3 + CH_3(+M) = C_2H_6(+M) \quad (R16)$$

$$CH_3 + CH_3 = H + C_2H_5 \quad (R17)$$

A validation of the methane submechanism was performed against to the laminar flame speed reported in literatures [84–90] and the oxidation of methane in jet-stirred reactor [91]. The predictions of the flame speed and the distributions of the species in methane oxidation are provided in the Supplementary Material.

3.2. Reactions of ethyl radical

The reactions of ethane largely produce ethyl radical, whose rate constants were referred to USC Mech II [35] in this model. Ethyl radical plays an important role in the combustion of meth-ane. The pressure-dependent decomposition of ethyl radical (R18) was theoretically studied by Miller and Klippenstein [92], which was very well validated against the low-pressure data. How-ever, Aul et al. [2] pointed out the over prediction of the reactivity, when this expression is adopted at 1–30 atm. A decrement of 30%of the low- and high-pressure limits was introduced in their work for accurate predictions of both the low- and high-pressure data. In this model, the value suggested by Aul et al. [2] was adopted, which was very different from the expression included in GRI Mech 3.0 [34] in either low- and high-pressure limits as well as the pres-sure dependency. (R19) is another efficient path during the conver-sion from ethyl to ethylene. Baulch et al. [73] evaluated the rate for (R19) as 4.21×10^{12}, while the value fitted from NIST database was 2.0×10^{12} in Aramco Mech 1.0 [36]. The former value was adopted in this model.

$$H + C_2H_4(+M) = C_2H_5(+M) \quad (R18)$$

$$C_2H_5 + H = C_2H_4 + H_2 \quad (R19)$$

Oxidation reactions between O atom and ethyl radical (R20), (R21), (R22) were updated in this model with the calculation of Harding et al. [75]. An additional reaction channel (R22) was introduced in their work, with a branching ratio of 0.21, 0.67 and 0.12 for (R20), (R21), (R22). The total reaction rate of $C_2H_5 + O$ varied in different investigations [75,83,93,94]. Comparatively high value was proposed by Tsang and Hampson [93] and Herron [94] (9.6×10^{13} and 1.3×10^{14}, respectively). Later studies suggested slower reaction rates, 6.62×10^{13} by Baulch et al. [83] and around 3.19×10^{13} in the work of Harding et al. [75]. The reaction between ethyl radical and molecular oxygen was also included in this model (R23) and (R24). Ethanol would be formed via the combination of ethyl and hydroxyl radicals, whose detailed kinetics is not discussed in this work.

$$C_2H_5 + O = CH_3CHO + H \quad (R20)$$

$$C_2H_5 + O = CH_3 + CH_2O \quad (R21)$$

$$C_2H_5 + O = C_2H_4 + OH \quad (R22)$$

3.3. The formation of benzene precursors

Acetylene is an important precursor in benzene formation. It is mainly formed via two pathways, the decomposition of vinyl radical and the isomerization of H_2CC carbene. Hydrogen abstraction reactions of ethylene produce vinyl radical (R25), (R26), (R27). Their rate constants are adopted from USC Mech II [35] and the work of Tsang [95]. And the successive unimolecular decomposition of vinyl radical (R28) is taken from USC Mech II [35]. The reactions contained in the other pathways (R29) and (R30) are also taken from USC Mech II.

$$C_2H_4 + H = C_2H_3 + H_2 \quad (R25)$$

$$C_2H_4 + OH = C_2H_3 + H_2O \quad (R26)$$

$$C_2H_4 + CH_3 = C_2H_3 + CH_4 \quad (R27)$$

$$C_2H_3(+M) = C_2H_2 + H(+M) \quad (R28)$$

$$C_2H_4(+M) = H_2 + H_2CC(+M) \quad (R29)$$

$$C_2H_2(+M) = H_2CC(+M) \quad (R30)$$

The recombination of C1 and C2 species could easily produce large amount of C3 intermediates, such as propane and propene, mainly via (R31)–(R33). Successive H abstraction reactions on these C3 molecules form C_3H_5 and C_3H_4 isomers. Anyway, propyne and allene, important benzene precursors in methane flames, are mainly yielded via the recombination of methyl radical and acetylene (R34) and (R35). Diau et al. [96] studied these reactions theoretically and emphasized the pressure effect on the reaction rate. Later experimental and theoretical investigations on the pyrolysis of propyne were performed by Davis et al. [97]. Their calculations agreed well with those of Diau et al. [96] and were supported by their experimental data. Therefore, the rate constants proposed by Davis et al. [97] for (R34) and (R35) were adopted in this model.

$$C_2H_2 + CH_3 = pC_3H_4 + H \quad (R34)$$

$$C_2H_2 + CH_3 = aC_3H_4 + H \quad (R35)$$

3.4. The formation of benzene, phenyl and benzyl radical

The self-combination reaction of propargyl radical (R36) and its addition reactions to propyne and allene (R37) and (R38) are major benzene (A_1) formation pathways in the flames investigated in this work. Various rate constants were recommended in previous studies, including the theoretical calculations [98,99], experimental measurements [100–102] and reasonable estimations [103,104]. The rate constant of (R36) in this model was referred to the theoretical investigation of Georgievskii et al. [98], which was modified by Hansen et al. [105] in their study on the premixed flames of C_3H_4 isomers. The addition reactions of propargyl radical to C_3H_4 isomers were proposed as important benzene formation pathways in the work of D'Anna and Kent [37]. Fulvene is one of the key iso-mers of benzene, which can rapidly isomerize to benzene via (R39) and (R40). The rate constants of (R39) and (R40) are referred to the theoretical calculation by Miller and Klippenstein [99] and Jasper and Hansen [51], respectively. The recombination of propargyl and allyl radicals (R41) was proposed for the formation of fulvene as a major benzene formation pathway in the work of Hansen et al. [105]. Other fulvene formation pathways were also included in this model, as well as other C3 + C3 and C4 + C2 benzene formation routes.

$$C_3H_3 + C_3H_3 = A_1 \quad (R36)$$

$$pC_3H_4 + C_3H_3 = A_1 + H \quad (R37)$$

$$aC_3H_4 + C_3H_3 = A_1 + H \quad (R38)$$

$$\text{Fulvene} = A_1 \quad (R39)$$

$$\text{Fulvene} + H = A_1 + H \quad (R40)$$

$$C_3H_3 + aC_3H_5 = \text{Fulvene} + 2H \quad (R41)$$

Phenyl radical (A_1-) is one of the important precursors of large aromatic species. It could be produced via the H abstraction from benzene and the recombination of small molecules. (R42) is a competitive channel of the self-combination reaction of propargyl radical. Its rate constant is derived from the work of Georgievskii et al. [98]. The reaction of propargyl and propadienylidene radicals (C_3H_2) was proposed in early kinetic studies [37,106,107], while was identified experimentally by Taatjes et al. [108] in premixed flames with the help of SVUV-PIMS. In this work, the rate constants of (R43) was taken from the work of Laskin et al. [107].

$$C_3H_3 + C_3H_3 = A_1\text{-} + H \quad (R42)$$

$$C_3H_2 + C_3H_3 = A_1\text{-} \quad (R43)$$

Benzyl radical, another PAH precursor, is mainly formed from toluene and phenyl radical (R46), (R47), (R48), (R49). The pressure-dependent rate constants of (R46) were taken from the theoretical investigation of Klippenstein et al. [109]. Their results have been experimentally validated in the shock tube pyrolysis of $C_6D_5CH_3$ by Sivaramakrishnan and Michael [110]. The H abstraction reaction of toluene by H and OH radicals can form benzyl radical via (R47) and (R48). The rate constant of (R47) was taken from the measurement of Oehlschlaeger et al. [111], which is slightly lower than the recommended value in the work of Baulch et al. [73]. Rate constant of (R48) was adopted from the measurements of Seta et al. [112] in this model. The pressure-dependent rate constant of (R49) calculated in the work of Klippenstein et al. [109] was used in this model, which results as another effective benzyl formation channel via its reverse reaction.

$$A_1CH_3(+M) = A_1CH_2 + H(+M) \quad (R46)$$

$$A_1CH_3 + H = A_1CH_2 + H_2 \quad (R47)$$

$$A_1CH_3 + OH = A_1CH_2 + H_2O \quad (R48)$$

$$A_1CH_2 + H = A_1\text{-} + CH_3 \quad (R49)$$

3.5. The formation of PAHs

Indene is mainly formed through the C6 + C3 (R50) and (R51) or C7 + C2 (R52) routes. Narayanaswamy et al. [113] estimated the rate of (R50) as 1.0×10^{13}. (R51) was studied with quantum chemical method in the work of Kislov and Mebel [114], however, the reaction rate constant was not reported in their study. This model adopts an estimated rate of this reaction by Matsugi and Miyoshi [54] and Zhang et al. [66] in their modeling studies on the pyrolysis of toluene. Meanwhile, Matsugi and Miyoshi [54] also estimated the rate constant of the recombination of benzyl (A_1CH_2) and acetylene (R52) based on the calculation of Kislov et al. [115] and Vereecken et al. [116,117] between 1000 and 4000 K. Another rate constant was provided by Vereecken et al. [116,117] within the temperature range of 200–2000 K. The estimation by Blanquart et al. [69] was used in this model, which agreed well with the latter value.

$$A_1\text{-} + C_3H_3 = C_9H_8 \quad (R50)$$

$$A_1 + C_3H_3 = C_9H_8 + H \quad (R51)$$

$$A_1CH_2 + C_2H_2 = C_9H_8 + H \quad (R52)$$

The reaction between of benzyl and propargyl radical is the most efficient formation pathway of naphthalene (A_2), which was proposed in previous modeling studies [37,38,40,69,118] as a global reaction of $A_1CH_2 + C_3H_3 = A_2 + 2H$. The reacting possibility was later confirmed by Matsugi and Miyoshi [44] in their quantum chemical calculation. Since it is not easy to restrict the uncertainty of the estimation of the global reaction rate, a four-steps simplified kinetic scheme (R53), (R54), (R55), (R56) provided in the work of Matsugi and Miyoshi [44] was adopted in this model. Methyleneindanyl ($C_9H_7CH_2$) radical is primarily formed via (R53). Its further decomposition could yield naphthalene or methyleneindene

($C_9H_6CH_2$). The latter intermediate can isomerize to naphthalene rapidly. The rate constants of (R54), (R55), (R56) were provided in Chebyshev polynomial form in [44]. Therefore, they were fitted into Arrhenius format in this work with the maximum error of 51%. The rate constant of (R53) was estimated as $5.0 \times 10^{13} e^{-4026/T}$ in this work, whose activation energy was the same as the estimation in the work of Richter and Howard [118].

$$A_1CH_2 + C_3H_3 = C_9H_7CH_2 + H \quad (R53)$$

$$C_9H_7CH_2 = C_9H_6CH_2 + H \quad (R54)$$

$$C_9H_7CH_2 = A_2 + H \quad (R55)$$

$$C_9H_6CH_2 + H = A_2 + H \quad (R56)$$

The decomposition of benzyl radical forms fulvenallyl radical (C_7H_5), which is another important naphthalene precursor. The combination of fulvenallyl and propargyl radicals (R58) results in a considerable naphthalene formation route according to our model. The rate constant of (R58) refers to the self-combination of propargyl radical [99], taking into account of the difference in the molecular symmetry between fulvenally and propargyl radicals. The addition of phenyl radical to vinylacetylene (R60) was adopted from the suggestion of Blanquart et al. [69]. This pathway was also recommended by Richter and Howard [118] in their review of aromatic growth pathways. The self-combination reaction of cyclopentadienyl radicals (R63) [37,40,46,69,118] and HACA mechanism were also included.

$$C_7H_5 + C_3H_3 = A_2 \quad (R58)$$

$$A_1\text{-} + C_4H_4 = A_2 + H \quad (R60)$$

R67 and (R68) are two main formation pathways of acenaphthylene (A_2R_5). The recombination of indenyl (C_9H_7) and propargyl radicals (R67) was proposed in previous PAH models [40,57,69]. The reactivity of indenyl radical was over-estimated by Blanquart et al. [69]. Therefore, the value for (R67) used in this model was one fifth of the estimation of Blanquart et al. [69] to achieve a reac-tion rate analogus to the values of (R36). Another important forma-tion pathway of acenaphthylene follows the HACA mechanism (R68), which was evaluated by Wang and Frenklach [38,39]. Fluo-rene ($C_{13}H_{10}$) was proposed to be mainly formed through the recombination of indenyl and vinylacetylene (R69) in this model. The rate of this reaction was estimated as 3.0×10^{11} in the work of Zhang et al. [66] and Li et al. [56]. Some formation pathways of other PAHs are also listed in Table 2.

$$C_9H_7 + C_3H_3 = A_2R_5 + 2H \quad (R67)$$

$$A_2\text{-} + C_2H_2 = A_2R_5 + H \quad (R68)$$

$$C_9H_7 + C_4H_4 = C_{13}H_{10} + H \quad (R69)$$

4. Numerical simulation methods

Laminar premixed and counter flow diffusion flames were calculated with OpenSMOKE [119], while laminar coflow flames were numerically simulated with laminarSMOKE [48,120,121]. The detailed information for the design of the software was introduced elsewhere [47,119]. The thermodynamic properties of species in the present model were referred to different databases [122] or previous models [33–35,41,69]. The transport properties of flame species were taken from the CHEMKIN transport database [123] or estimated following the procedure described in [38]. Both Fickian and thermal diffusion [124] were taken into account in the simulation of all the flames. The radiation of the major flame species [125] was considered only in the laminarSMOKE simulations.

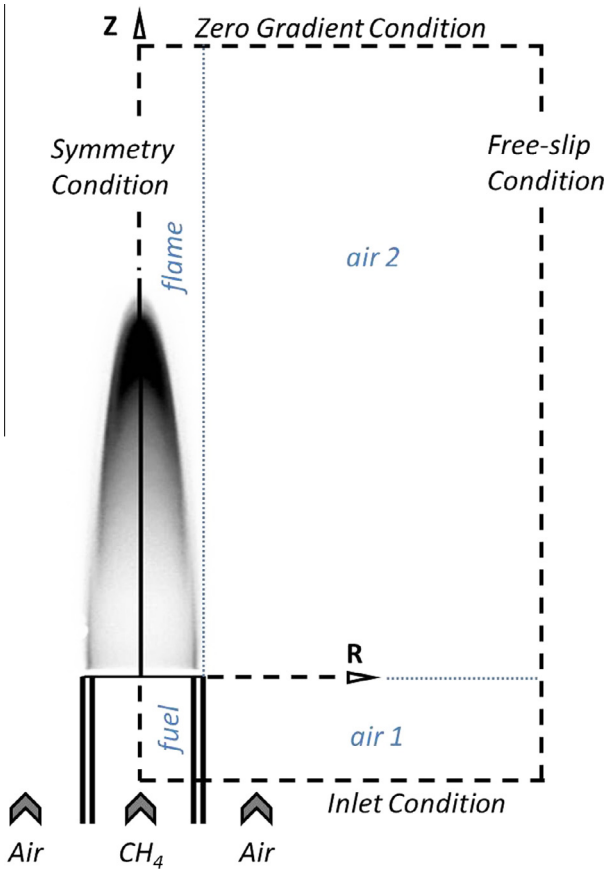

Fig. 1. Schematic representation of the burner and flame, with coordinate axes and computational domain boundaries (not drawn in real scale).

Figure 1 presents a detailed boundary condition of the control volume adopted in present CFD simulation of coflow flames. The fuel stream was assumed at 300 K with a parabolic inlet velocity profile, while the coflow air was imposed at ambient temperature with a flat velocity profile. The inlet boundary of fuel mixture and air flow was fixed according to the conditions in Table 1. Because of the axial symmetry of the system, the numerical calculations were performed on a stretched, two-dimensional, rectangular domain, with length of 297 mm and width of 58 mm. Along the centerline, we adopted a finer numerical grid near the exit of the burner. Similarly, along the radial direction uniform cell spacing is adopted to describe the flame region, while coarser grid points are used in air flow. Considering the balance between the accuracy of numerical calculation and the cost of computational time, a mesh with 9504 cells (144×66 cells) was found fine enough for the purpose of this work.

5. Result and discussion

In this section, validations were performed to various experimental data obtained from different kind of laminar methane flames (Table 1) with detailed chemical kinetic analysis, including premixed flames [22–24], counter flow diffusion flame, and coflow diffusion flames. The decomposition of methane, the recombination of small molecules, and the formation of benzene and PAHs will be discussed individually in the following, taking into account the influence of different flame conditions on these reaction pathways. The common kinetics and the discrepancies among different flame conditions will be generalized and compared.

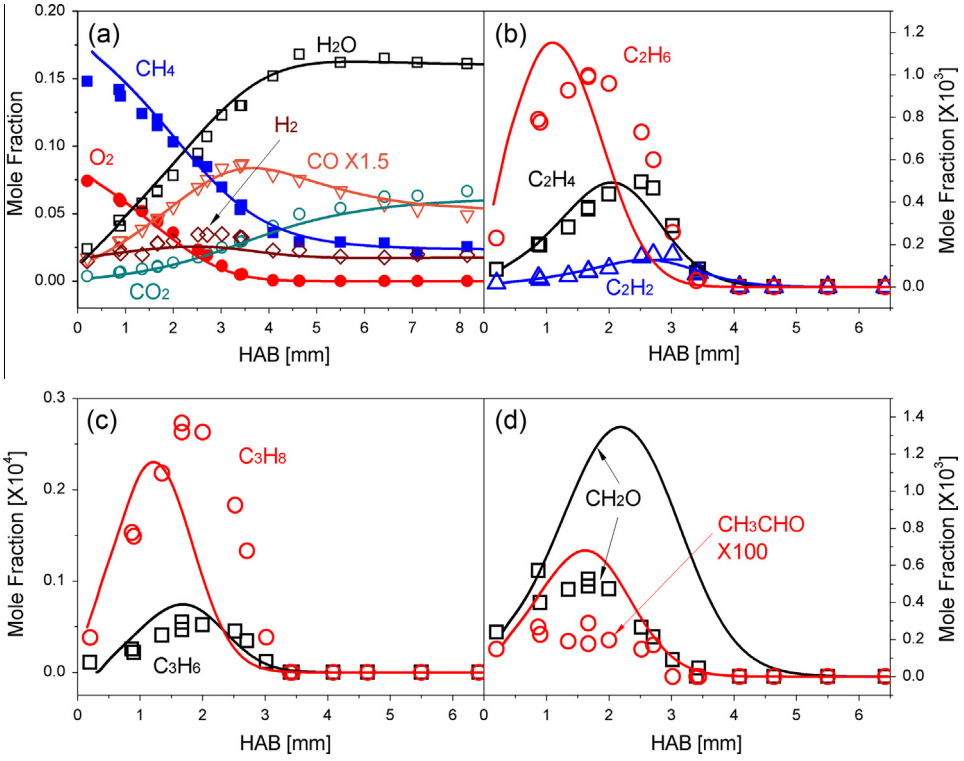

Fig. 2. Mole fraction comparison of experimental measurements (symbols) and numerical predictions (lines) of major and intermediate species in stoichiometric methane flame (*PF1*) [22].

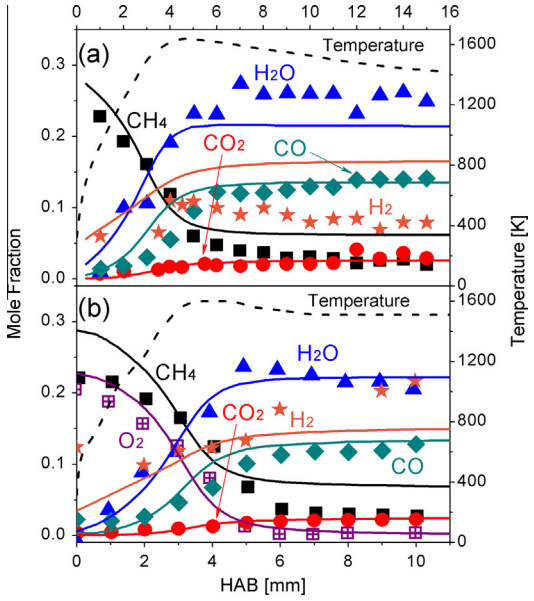

Fig. 3. Mole fraction comparison of experimental data (symbols) and numerical predictions (lines) of major species in fuel rich (ϕ = 2.6) premixed methane flame. Experimental data in (a and b) refers to *PF2* [24] and *PF3* [23]. Temperature profile used in simulation of (a) is adopted from the smoothed profile in Slavinskaya and Frank [40].

The model predictions of flame species in low pressure premixed stoichiometric methane flame (*PF1*) are presented in Fig. 2. The experimental data of this flame was obtained from the work of Tran et al. [22]. Castaldi et al. [24] and Melton et al. [23] diagnosed a fuel-rich methane flame in atmospheric pressure (*PF2* and *PF3*) separately with the same experimental apparatus, while very similar flame conditions were controlled in their experiments. The model predictions of the major species (CH_4, O_2, H_2, H_2O, CO, and CO_2) in *PF2* and *PF3* are presented in Fig. 3; whilst the predictions of C2–C4 intermediates are displayed in Fig. 4. In Fig. 3, the distribution of the O_2, H_2O, CO, and CO_2 are well captured, except CH_4 and H_2. The deviations were ascribed to the element balances of C and H in the experimental results (see Supplementary Material).

The counter flow diffusion flame measured by Lim et al. [60] was numerically investigated in present work (*OF1*). Figure 5 compares the main flame species observed in *OF1* and predicted by the model. Four methane coflow diffusion flames varied by different diluting ratios of nitrogen were investigated in this work (*CF1–CF4*). In order to show a typical result of this validation, Fig. 6a shows the predicted mole fraction of propyne in *CF4* in radial direc-tion at various flame heights (HAB), whilst Fig. 6b compares mea-sured and simulated results of propyne along the centerline of *CF4*. Figure 7 shows the measured and predicted mole fraction profiles of major flame species in *CF4*. The comparisons of the flame struc-tures of *CF1–CF3* can be found in the Supplementary Material.

5.1. Methane decomposition and small molecule aggregation

Fuels always decompose via their specific pathways depending on the particular molecular structures and the operating conditions. Methane, that is the simplest hydrocarbon, has four C–H bonds with identical dissociation energy of 105 kcal/mol. Unimolecular decomposition (R1) does not provide an efficient way in the decomposition of methane. H abstraction reactions by free rad-icals (R2), (R3), (R4), such as H and OH radicals, dominate its consumption producing the only intermediate, methyl radical. The reaction flux diagrams of the decomposition and oxidation of methane in different flames are presented in Fig. 8. Over 85% of methane is consumed via H abstraction reactions of different free radicals, while their contributions vary in the different flame

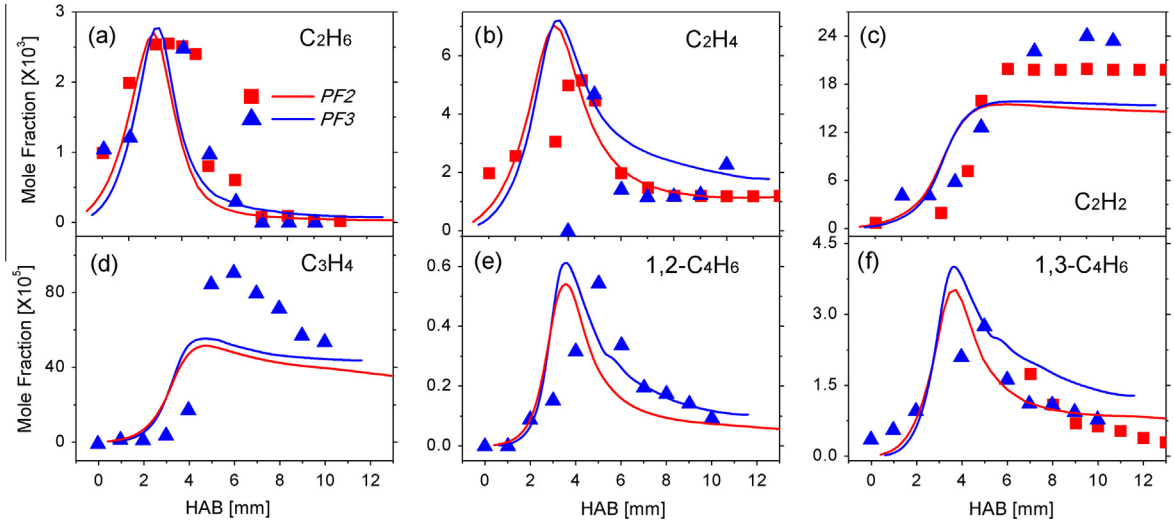

Fig. 4. Mole fraction predictions of intermediates in fuel rich (ϕ = 2.6 for both *PF2* [24] and *PF3* [23]) premixed methane flames. Lines and symbols denote the modeling results and the experimental data. In order to minimize the influence of experimental uncertainty on modeling studies, the mole fractions of combustion intermediates in both flames are plotted in the same scale in the figure.

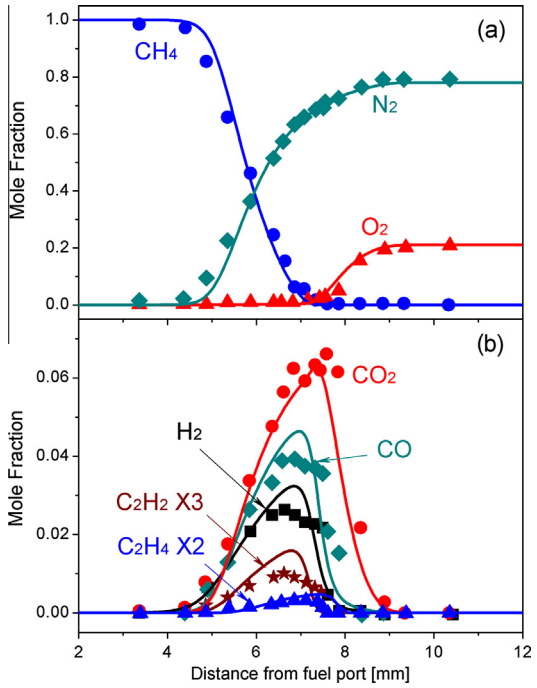

Fig. 5. Modeling predictions of the flame structure of the counter flow flame (*OF1*) [60], symbols denote experimental data and lines for numerical predictions.

conditions. Identical contribution of H and OH radicals can be observed in near stoichiometric premixed flames (Fig. 8a), while the contribution of OH radical reduces with the increase of the flame equivalent ratio (Fig. 8b). A much higher contribution of H atom in abstracting hydrogen from methane can be observed in diffusion flame (Fig. 8c and d), because of the more efficient diffusion of H atom over OH radical from the flame front toward the fuel side.

During the successive reactions, the recombination of methyl radical yielding ethane (R16) is the major consumption pathway in rich premixed flames, while the reactions with O and OH radi-cals (R5), (R6), (R7), (R8), (R9), (R10), (R11) dominate in lean and stoichiometric flames. As shown in Fig. 8a, the self recombination of methyl radicals (R16) represents only 8.2% in the consumption of methyl radical in stoichiometric flame (*PF1*), while most of eth-ane would return to methyl via the decomposition of ethyl radical (R17). On the contrary, the recombination of small molecules is the main pathway in rich flames (*PF2*). As shown in Fig. 8b, 44.2% of methyl radical forms ethane via (R16), while 6.2% via (R17) yield-ing ethyl radical. The competition of these two channels (R16) and (R17) in diffusion flames is very different from that in rich pre-mixed flames, as shown in Fig. 8c and d. H atom radical, whose concentration controls the reaction rate of the whole flame system, is only marginally formed in the fuel side of diffusion flames. (R16), a termination reaction forming ethane, whose further decomposi-tion is dependent on the concentration of free radicals, therefore is not as important as that in premixed flames. Meanwhile, (R17), a chain propagation reaction, that produces H atom radical, provides a significant contribution in the recombination of methyl radical. As shown in Fig. 8d, identical contributions of (R16) (18.1%) and (R17) (16.2%) were observed in *CF2*. Ethyl radical subsequently produces acetylene in a few H abstraction and β-scission steps. The model predictions of C2 species in different flame conditions are presented in Figs. 2b, 4a–c, 5b and 9, with a good agreement with the experimental data.

Propane and propene are formed through the combination of ethyl and vinyl radicals with methyl radical. Their further decomposition reactions are not the main formation pathways of C_3H_4 isomers in these conditions. As shown in Fig. 8b, the recombination between acetylene and methyl radical (R34) accounts for 8.4% in the consumption of methyl radical and provides a contribution of over 90% in the formation of propyne in *PF2*. This pathway shows a higher importance in the consumption of methyl radical in coflow diffusion flames (Fig. 8d), because of the lack of OH oxidiz-ing radical in the pyrolytic centerline of the flame. (R34) is also the dominant formation pathway of propyne in coflow diffusion flames [48,61,65]. Propyne can isomerize to allene, while finally propargyl radical is formed through the decomposition of C_3H_4 iso-mers. The model predictions of C3 species are presented in Figs. 2c, 4d and 10. Propargyl radical is over-predicted by a factor of 2 in all four coflow flames. Annihilation effect is considered as its major cause of this deviation [126], which would be very detrimental in probe sampling in atmospheric pressure.

C4 species are not important benzene precursors in methane flames. Among the predictions presented in Figs. 4e, 4f and 11, the amounts of butadiene isomers agree well between measure-

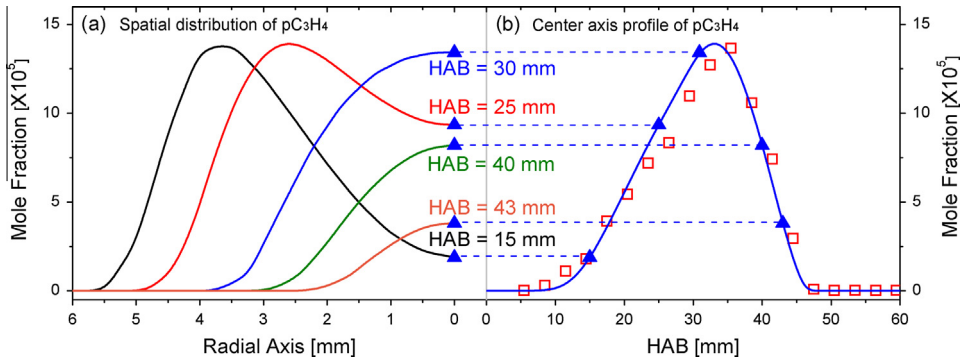

Fig. 6. (a) Spatial distribution of propyne in the CFD simulation of *CF4*; (b) comparison between experimental measurements and modeling predictions of propyne along the flame center line. Blue line denotes the numerical result and red symbol denotes the experimental data. (For interpretation of the references to color in this figure legend, the reader is referred to the web version of this article.)

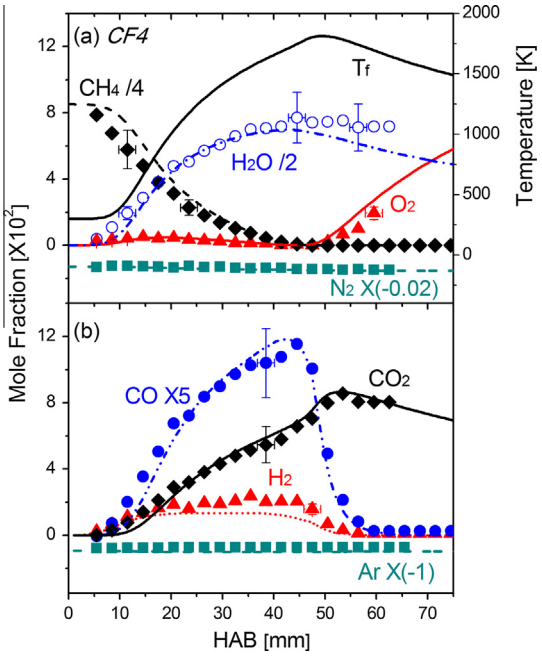

Fig. 7. Coflow flame structure along the centerline of *CF4*. Symbols and lines denote experimental measurements and modeling predictions. Calculated flame temperature profile is presented with black solid line in (a). The mole fractions of N_2 and Ar are multiplied by −0.02 and −1 respectively, for a clear plotting of their data in the same scale with other species.

ments and predictions in premixed and coflow flames, while their peak positions are not well captured. Because of the large quantity of methyl radical in this flame condition, the addition reactions of methyl radical to propyne and allene are the major formation channels of 1,3-butadiene. The subsequent H abstraction reactions of butadiene isomers form vinylacetylene and butadiyne. As shown in Fig. 11, vinylacetylene is under-predicted by around 25%; butadiyne is perfectly predicted in *CF1*, while under-predicted by 50% in *CF4*.

5.2. The formation of benzene and PAH precursors

Benzene formation pathways have been studied extensively in flames, including the addition of C4 radicals to acetylene (even routes) [39,127] and the combination of C3 species (odd routes) [37,68,98,99,104,128,129]. Other formation routes are also included in the model, such as the recombination of methyl and cyclopentadienyl radicals [130,131] and the dehydrogenation of cyclohexane [132]. The modeling predictions of benzene are presented in Figs. 12a and 13 with a good agreement with its formation tendency in fuel rich premixed flames and coflow diffusion flames.

In the previous studies of methane flames, different conclusions were achieved because of their different flame conditions and the deviation of theoretical and experimental information on benzene formation [27,37,40,47,48]. As suggested by D'Anna and Kent [37] and Slavinskaya and Frank [40] in their studies on laminar meth-ane flames, the self-combination of propargyl radical (R30) was the dominant benzene formation pathway in methane flames. Sim-ilar conclusions are achieved in this work. As shown in Fig. 14, in either rich premixed flames (*PF2*), counter flow diffusion flames (*OF1*) and coflow diffusion flames (*CF2*), (R36) provides a contribution over 35%. The addition of propargyl radical to C_3H_4 isomers are also important pathways in benzene formation. A large quantity of propyne is formed through (R34) in different flames, which plays as not only an important producer of propargyl radical, but also a direct benzene formation contributor. Fulvene is an important isomer of benzene, which can be also formed via the recombination of propargyl radicals [99,104]. The isomerization reaction of fulvene to benzene is an additional benzene formation pathway in laminar methane flames. The importance of even pathways is not significantly observed in laminar methane flames investigated in this work. As concluded by Zhang et al. [133] in their comprehensive investigation on the fuel dependence of benzene pathways, benzene precursors for C4 + C2 pathways, such as C_4H_5 and C_4H_3 radicals, cannot be easily formed in methane flames, compared to flames fed with C2 hydrocarbons.

Sensitivity analysis was performed in the flame conditions of *PF2* and *OF1*, presented in Fig. 15. Obviously, the reactions that accelerate the whole combustion system should have positive sensitivity coefficients in premixed flames, such as $H + O_2 = O + OH$, $O + H_2 = H + OH$, and $CH_4 + O = CH_3 + OH$ (R4). The C3 + C3 benzene formation pathways present positive sensitivities in both premixed and diffusion flames. Due to the difference in flame conditions, there are huge discrepancies in the spatial distributions of free rad-icals and the reaction possibilities between premixed and diffusion flames. Reactions between locally produced radicals have much more opportunities for recombination reactions in diffusion flames, because of the difficulty in the diffusion of free radicals. Therefore, (R17) and (R34) are more sensitive in diffusion flames. On the other hand, there are more oxidative radicals in premixed flame, which lead to negative sensitivity coefficients for the oxida-tion reactions of benzene precursors.

The predictions of cyclopentadiene, toluene, phenylacetylene and styrene in fuel rich premixed flames and coflow diffusion

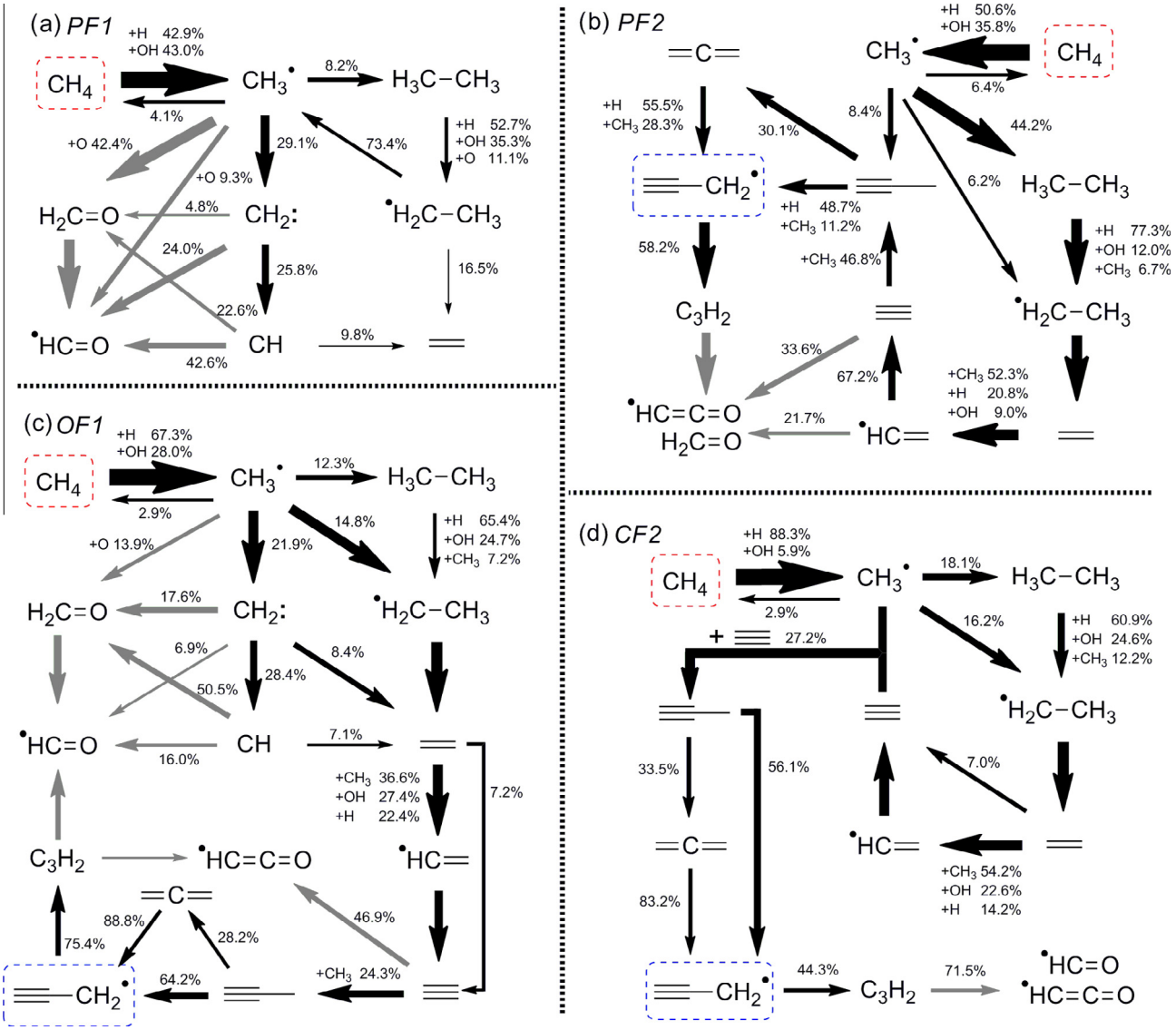

Fig. 8. Main reaction paths in methane flames. The thickness of the arrows is proportional to the mass fluxes of the reactions. The conversion rates marked aside the arrows is the normalized rate of production values integrated across the flame front for *PF1*, *PF2* and *OF1*, and along the centerline axis of the flame for *CF2*. Gray arrows highlight the oxidation pathways.

flames are compared in Figs. 12, 13 and 16. Small quantity of cyclopentadiene is formed in coflow diffusion flames, which reveals that cyclopentadienyl radical is in low concentration. Since the reaction between cyclopentadienyl and propargyl radicals is an important formation pathway of styrene, its concentration is also very low in these flames. Benzene is the controlling species for the formation of other aromatic hydrocarbons, since it is the main provider of phenyl radical in flames. Phenylacetylene is mainly formed via the addition of phenyl radical to acetylene. The recombination of methyl radical and phenyl radical forms toluene and benzyl radical (R44) and (R49), as shown in Fig. 17. Reaction (R49) plays a more efficient role in the competition of these two channels in both premixed and diffusion flames. The substitution of methyl radical to the H atom on benzene (R45) provides an efficient route for the formation of toluene. Its contribution is about 5–10 times higher than that of (R44) in *PF3* and *CF2*. The further decomposition product of toluene (R46) and (R47) is benzyl radical, which is a resonantly stabilized radical and thus an important PAH precursor in methane flames.

5.3. Aromatic growth process: from one ring to three rings

Indene and naphthalene are the key species in PAH growth process. Both their mole fractions were measured experimentally in previous methane flame investigations [23,24] and reproduced by this model, as shown in Fig. 12 (*PF2* and *PF3*). The experimental and modeling results in coflow diffusion flames are presented in Fig. 18, with the influence of the nitrogen dilution on their forma-tions. Mole fractions of indene and naphthalene in *CF4* are only one fifth of those in *CF1*. The uncertainties in the measurements of coflow diffusion flames are ±50% and a factor of 2 for indene and naphthalene respectively, while they were in a factor of 2 in the premixed flames [23,24]. The model performs well in the predictions of indene and naphthalene in *PF2*, *PF3* and *CF1*, but slightly under-predicts naphthalene formation in *CF2*–*CF4*.

According to the aromatic formation routes in Fig. 17, over 21% of benzene reacts with propargyl radical (R51) in *CF2* to form indene, while this reaction provides a minor contribution in *PF2*. Compared to the addition of benzyl radical to acetylene (R52),

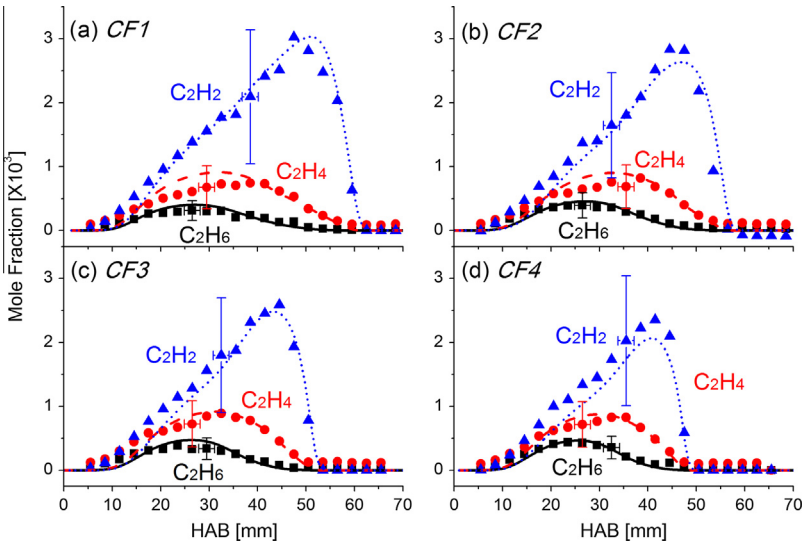

Fig. 9. C2 species (C_2H_2, acetylene; C_2H_4, ethylene, C_2H_6, ethane) in *CF1–CF4* (N_2 dilution: 50% for *CF1*, 55% for *CF2*, 60% for *CF3* and 65% for *CF4*), symbols and lines denote the experimental and numerical results.

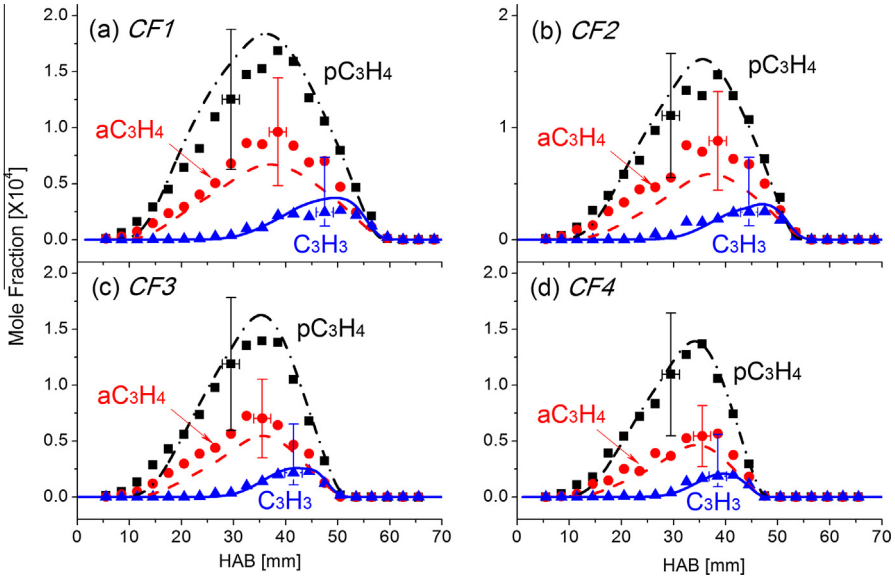

Fig. 10. C3 species (pC_3H_4, propyne; aC_3H_4, allene; C_3H_3, propargyl) in *CF1–CF4* (N_2 dilution: 50% for *CF1*, 55% for *CF2*, 60% for *CF3* and 65% for *CF4*), symbols and lines denote the experimental and numerical results. For a clear illustration of the over-prediction of propargyl radical in quantity, its simulation results are divided by a factor of 2 to agree with the experimental data.

(R51) is another significant formation pathway in coflow diffusion flames. The contributions of (R51) and (R52) in the indene formation in *CF2* are much higher than that of the recombination of phenyl and propargyl radicals (R50). The low concentration of H and OH radicals in the centerline of coflow flame can explain the importance of reaction (R51), since phenyl radical cannot be formed sufficiently via the H abstraction of benzene. On the other hand, propargyl radical, that is a resonantly stabilized free radical, is produced and accumulated in the center of coflow flames. Its high concentration favors reaction (R51). On the contrary, in premixed flames, phenyl and benzyl radicals are easily formed via H abstraction of benzene and toluene by H and OH radicals. Therefore, indene is dominantly formed from benzyl radical via (R52) in *PF3*, meanwhile a slight contribution comes from (R50).

As shown in Fig. 18, there are two peaks in the predictions of indene in all the coflow flames, which are not clearly observed in experimental data. Local ROP analysis of indene was performed in *CF1* at HAB = 27.5 mm to figure out the exact reaction contribut-ing for the first peak. The analysis shows that (R52) is the major formation pathway at this flame height, with a contribution around 65%. The rate constants of (R52) used in this model was referred to Blanquart et al. [69], whose activation energy could be underestimated.

Sensitive reactions that significantly impact the formation and the decomposition of indene in fuel rich premixed flame (*PF2*) and diffusion flame front (*OF1*) are listed in Fig. 19. (R51) and (R52), the major indene formation reactions, are unexpectedly not the most sensitive reactions in fuel rich premixed flames. The recombination of propargyl radical (R36) is the most sensitive one, besides the reaction of H atom with oxygen molecule. Since benzene is the dominant basis of PAH growth, the reactions producing benzene and benzene precursors also present positive

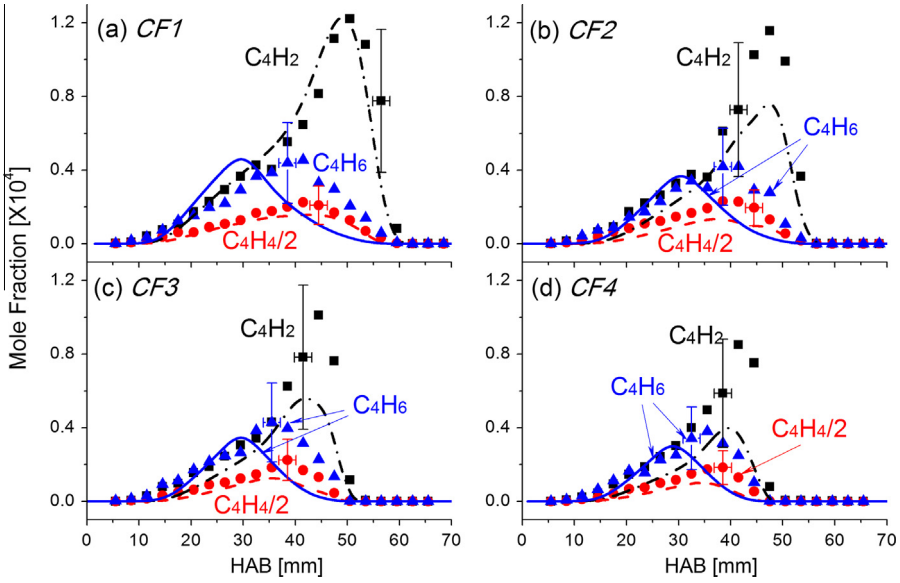

Fig. 11. C4 species (C4H6, butadiene; C4H4, vinylacetylene; C4H2, butadiyne) in *CF1–CF4* (N_2 dilution: 50% for *CF1*, 55% for *CF2*, 60% for *CF3* and 65% for *CF4*), symbols and lines denote the experimental and numerical results.

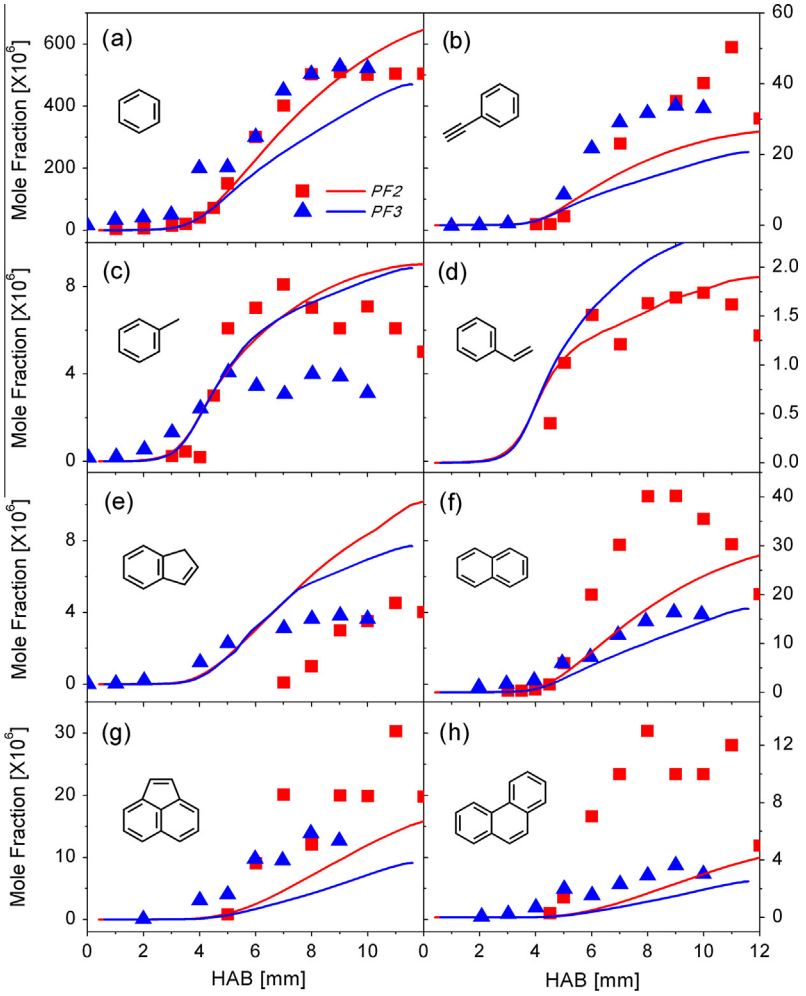

Fig. 12. Mole fraction predictions of aromatic species in fuel rich ($\phi = 2.6$) premixed methane flame. Lines and symbols denote the modeling results and the experimental data.

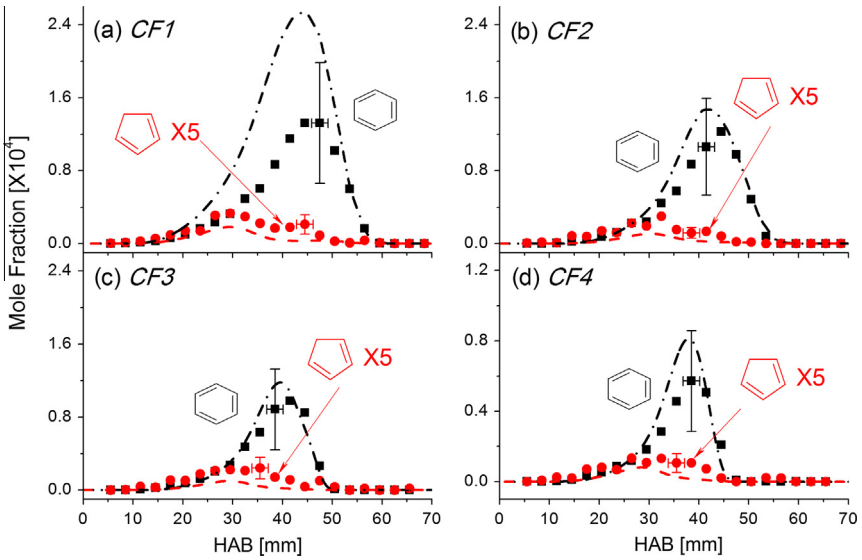

Fig. 13. C5 and C6 species in *CF1–CF4* (N_2 dilution: 50% for *CF1*, 55% for *CF2*, 60% for *CF3* and 65% for *CF4*), symbols and lines denote the experimental and numerical results.

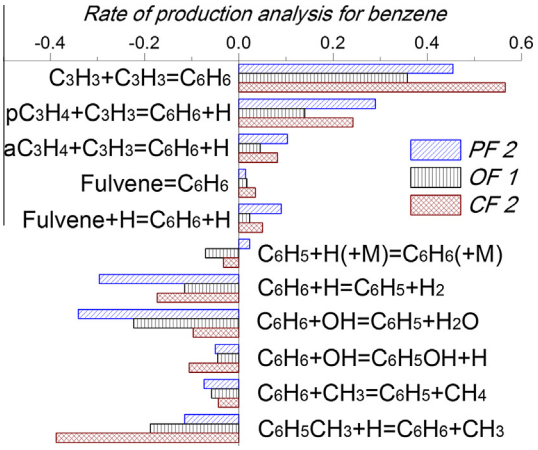

Fig. 14. Rate of production analysis of benzene in *PF2*, *OF1* and *CF2*.

coefficients, while the consumption reactions of them exhibit negative values. Indenyl radical is the dominant decomposition product of indene. Therefore, indene is also very sensitive to the reactions between indenyl radical and other small molecules that provide large contributions in its consumption.

Naphthalene is mainly formed through three pathways in either premixed or diffusion flames. In the present model, even route contains the addition of vinyl radical to phenylacetylene (R66), the addition of ethynyl radical to styrene, and the HACA pathways suggested by Wang and Frenklach [39]. The odd route mainly consists of two reaction pathways (R53), (R54), (R55), (R56), (R58), the addition of propargyl radical to benzyl and fulvenallyl radicals (C_7H_5). Because of the low mole fraction of styrene observed experimentally and numerically in premixed and diffusion flames (Figs. 12d and 16), its contribution to the formation of naphthalene is negligible. HACA mechanism proposed the addition of acetylene to the C_8H_5 radical, which could be formed via the H abstraction of phenylacetylene. However, its contribution is also in quite small proportion. (R66) is the main even reaction route, as shown in Fig. 17, providing contributions of 12% and 2.1% in the formation of naphthalene in *PF2* and *CF2*, respectively. The major contributors to the formation of naphthalene in methane flames are the odd routes, which are based on the reactions of resonantly stabilized free radicals. There are obviously two advantages over HACA mechanism. The resonantly stabilized free radicals have longer residence times than other radicals, while they are more active than stable species. (R53) and (R58) provide the main naphthalene formation contributions of 62.7% and 15.9% in *PF2*, 74.3% and 20.9% in *CF2*, respectively. The self-combination of cyclopentadienyl radical is considered as one of the major routes of naphthalene formation in previous studies on PAH formation [46,67]. However, according to present modeling study, it is a minor pathway in methane flames due to the rather low mole fractions of cyclopentadienyl

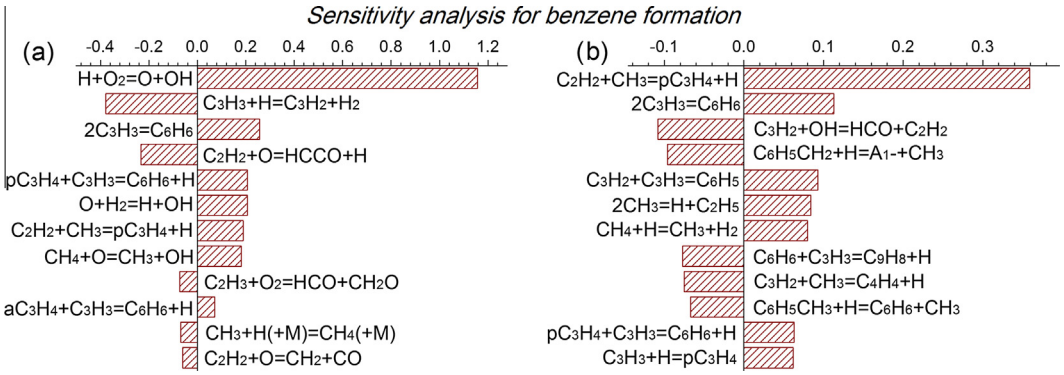

Fig. 15. Sensitivity analysis for benzene formation in (a) *PF2* and (b) *OF1*.

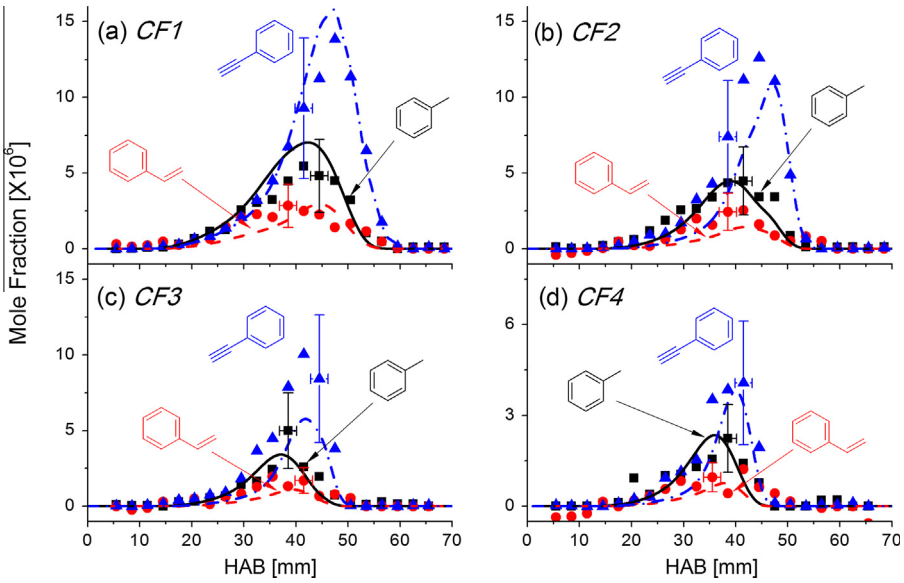

Fig. 16. C7 and C8 species in *CF1–CF4* (N_2 dilution: 50% for *CF1*, 55% for *CF2*, 60% for *CF3* and 65% for *CF4*), symbols and lines denote the experimental and numerical results.

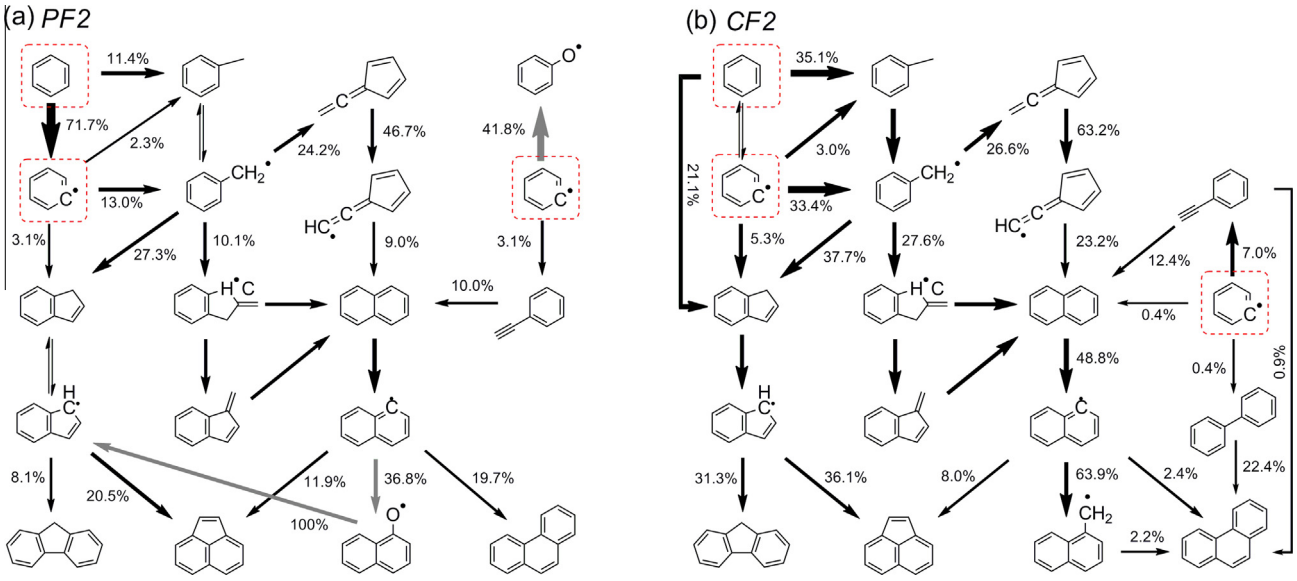

Fig. 17. Main PAH formation paths in methane flames. The thickness of the arrows is proportional to the mass fluxes of the reactions, and the conversion rates are marked beside them. Gray arrows highlight the oxidation pathways.

radical, which can be speculated from the mole fraction of cyclopentadiene in Fig. 15.

Figure 20 presents a sensitivity analysis of naphthalene formation in *PF2* and *OF1*. Reactions that form naphthalene and its precursors reveal positive sensitivity coefficients in both premixed and diffusion flames. Among the reactions with negative coeffi-cients, rapid consumption reactions of C_3H_2 and acetylene are very sensitive, because C_3H_2 is very important in the oxidation of propargyl radical, while acetylene is a major provider of propargyl radical. Combined with the information of ROP analysis, propargyl radical is the key intermediate in formation pathway of naphthalene. It is also interesting to observe that the decomposition reaction of methane significantly affects the formation of naphthalene. The difference in the H abstraction rate of O and H radicals in (R4) and (R2) corresponds to the discrepancy of premixed and diffusion flames.

Fluorene ($C_{13}H_{10}$), biphenyl (P_2) and acenaphthylene (A_2R_5) were also observed in coflow methane flames (*CF1–CF4*). Their production is significantly influenced by the nitrogen dilution, as shown in Fig. 21. Experimental data of biphenyl ($C_{12}H_{10}$) in *CF4* is not plotted in this figure, due to the weak signals in mass spec-tra. Large uncertainty (around a factor of 3) may be introduced in the data evaluation process, especially in *CF4* diluted 65% nitrogen. Acenaphthylene and phenanthrene ($C_{14}H_{10}$) were observed in fuel rich premixed flame (*PF2* and *PF3*) and measured with large uncertainty (Fig. 12). In both premixed and coflow diffusion flames, indenyl and naphthyl radicals are the main precursors of larger aromatic species, which are the dominant products of indene and naphthalene. The following discussion on the formation of large aromatic hydrocarbons will take *CF2* as an example, since the reaction pathways are quite similar to other flames. The addition of propargyl and vinylacetylene on indenyl (R67) and (R69) are the

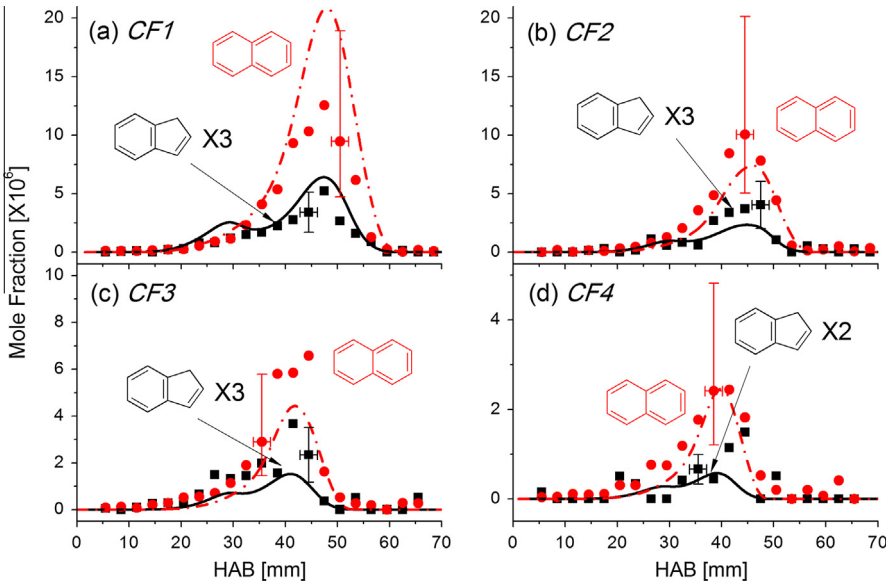

Fig. 18. C9 and C10 species in *CF1–CF4* (N_2 dilution: 50% for *CF1*, 55% for *CF2*, 60% for *CF3* and 65% for *CF4*), symbols and lines denote the experimental and numerical results.

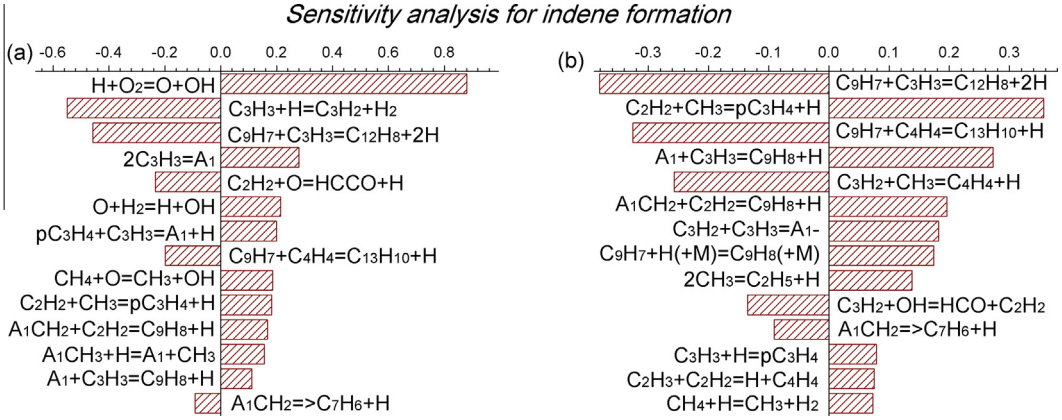

Fig. 19. Sensitivity analysis for indene formation in (a) *PF2* and (b) *OF1*.

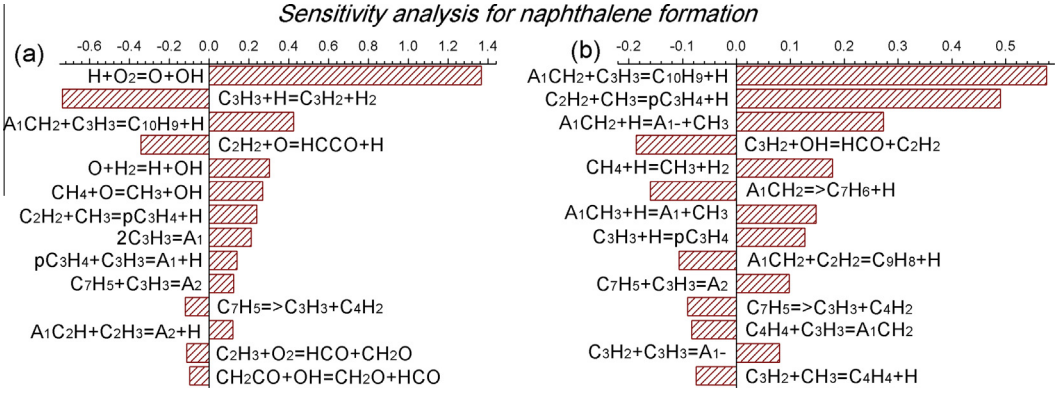

Fig. 20. Sensitivity analysis for naphthalene formation in (a) *PF2* and (b) *OF1*.

major formation pathways of acenaphthylene and fluorene, respectively. (R67) was proposed in the former studies of Slavinskaya et al. [70] and was the dominant formation pathway of acenaphthylene in their model. The addition of naphthyl radical to acetylene (R68) is another formation pathway of acenaphthylene. This reaction was previously proposed by Wang and Frenklach [39] in their investigation of PAH formation in acetylene and ethyl-ene flames. Shulka and Koshi [134,135] reviewed this reaction and

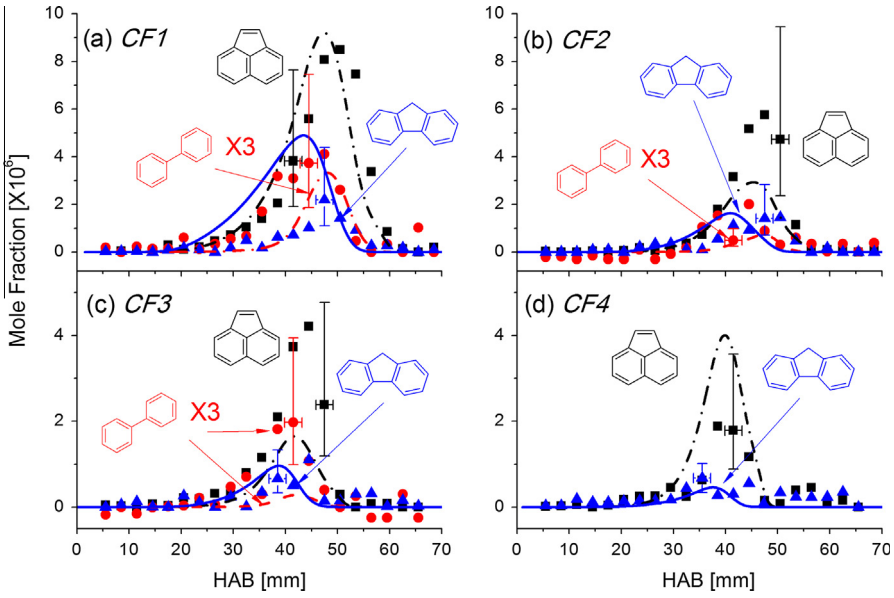

Fig. 21. C12 and C13 species in *CF1–CF4* (N_2 dilution: 50% for *CF1*, 55% for *CF2*, 60% for *CF3* and 65% for *CF4*), symbols and lines denote the experimental and numerical results.

proposed the further HACA based mechanism of acenaphthylene as a novel route for the formation of fluoranthene. Phenanthrene was also observed in coflow flames (its mole fractions are provided in the Supplementary Material). It is mainly formed from naphthyl radical. Biphenyl is an unstable product of the combination of phenyl radical, which mainly decomposes in the inverse direction after its formation.

6. Conclusions

Combining previous experimental investigations of methane premixed and counter flow diffusion flames with coflow diffusion flames diagnosed in this work, comprehensive modeling studies on laminar methane flames were performed with OpenSMOKE and laminarSMOKE codes. A detailed kinetic model extended to aromatic growth mechanism allows a good characterization of methane oxidation, small molecule aggregation processes, benzene and PAH formation mechanisms. The comparison between the model and the different methane flames showed that it varied significantly in different combustion conditions of the decomposition of methane, the formation of small species and their successive reactions leading to the formation of aromatic species. In premixed flames, because of the overlap of the free radicals and stable species in spatial distribution, all intermediate species gives a significant contribution to the reaction system. On the contrary, active free radicals cannot efficiently diffuse from flame front to the fuel or oxidizer sides in diffusion flames. The comparison of the reaction pathways in premixed and diffusion flames shows that the local production of free radicals plays a different role and controls the competition between alternative reaction pathways by influencing the possibility of reactions. In fact, a coflow diffusion flame is enveloped by a flame front, which leads to the merely absence of oxidative species in the center of the flame. Therefore, benzene formation and PAH growth reactions are the only effective reaction pathways for flame intermediates in that region.

Resonantly stabilized free radicals, such as propargyl, phenyl, and benzyl radicals, are main PAH precursors, as well as indenyl and naphthyl radicals for large PAHs. The reactions of these radicals with small hydrocarbon intermediates or their recombination are the most efficient aromatic growth pathways. Considering the balance of the reactivity and residence time of the intermediate species in the flames, resonantly stabilized free radicals, which are more active than stable intermediates in chemical reactions and have longer residence time than active free radicals, have much more opportunity to be involved in the PAH formation mechanism. Further theoretical investigation and accurate experimental measurements on the growth of large PAH species are anyway demanded to reproduce their formation and growth accurately under a wide range of combustion conditions.

Acknowledgments

Authors are grateful for funding supports from National Basic Research Program of China (973 Program) (2013CB834602), Natural Science Foundation of China (U1332208, 51127002) and Chinese Academy of Sciences.

Appendix A. Supplementary material

Supplementary data associated with this article can be found, in the online version.

References

[1] J.X. Zhang, E.J. Hu, Z.H. Zhang, L. Pan, Z.H. Huang, Energy Fuels 27 (2013) 3480–3487.
[2] C.J. Aul, W.K. Metcalfe, S.M. Burke, H.J. Curran, E.L. Petersen, Combust. Flame 160 (2013) 1153–1167.
[3] Y.J. Zhang, Z.H. Huang, L.J. Wei, J.X. Zhang, C.K. Law, Combust. Flame 159 (2012) 918–931.
[4] L.J. Spadaccini, M.B. Colket, Prog. Energy Combust. Sci. 20 (1994) 431–460.
[5] E. Albin, H. Nawroth, S. Goke, Y. D'Angelo, C.O. Paschereit, Fuel Process. Technol. 107 (2013) 27–35.
[6] L. Selle, T. Poinsot, B. Ferret, Combust. Flame 158 (2011) 146–154.
[7] L.K. Tseng, M.A. Ismail, G.M. Faeth, Combust. Flame 95 (1993) 410–426.
[8] E. Ranzi, A. Frassoldati, R. Grana, A. Cuoci, T. Faravelli, A.P. Kelley, C.K. Law, Prog. Energy Combust. Sci. 38 (2012) 468–501.
[9] C. Keramiotis, G. Vourliotakis, G. Skevis, M.A. Founti, C. Esarte, N.E. Sánchez, A. Millera, R. Bilbao, M.U. Alzueta, Energy 43 (2012) 103–110.
[10] H. Schwarz, M. Geske, C. Franklin Goldsmith, R. Schlögl, R. Horn, Combust. Flame 161 (2014) 1688–1700.
[11] R. Mevel, S. Javoy, K. Coudoro, G. Dupre, C.E. Paillard, Int. J. Hydrogen Energy 37 (2012) 698–714.
[12] C. Tanh Le, P. Dagaut, Proc. Combust. Inst. 32 (2009) 427–435435.
[13] T. Le Cong, P. Dagaut, Energy Fuels 23 (2009) 725–734.
[14] T. Le Cong, P. Dagaut, G. Dayma, J. Eng. Gas Turb. Power 130 (2008) 041502.
[15] Y. Hidaka, K. Sato, Y. Henmi, H. Tanaka, K. Inami, Combust. Flame 118 (1999) 340–358.
[16] W.C. Gardiner, S.M. Hwang, M.J. Rabinowitz, Energy Fuels 1 (1987) 545–549.

[17] P. Roth, T. Just, Proc. Combust. Inst. 20 (1984) 807–818.
[18] R.J. Cattolica, S. Yoon, E.L. Knuth, Combust. Sci. Technol. 28 (1982) 225–239.
[19] E.R. Ramer, J.F. Merklin, C.M. Sorensen, T.W. Taylor, Combust. Sci. Technol. 48 (1986) 241–255.
[20] C.K. Westbrook, F.L. Dryer, Combust. Flame 37 (1980) 171–192.
[21] M. Alfe, B. Apicella, J.N. Rouzaud, A. Tregrossi, A. Ciajolo, Combust. Flame 157 (2010) 1959–1965.
[22] L.S. Tran, P.A. Glaude, R. Fournet, F. Battin-Leclerc, Energy Fuels 27 (2013) 2226–2245.
[23] T.R. Melton, A.M. Vincitore, S.M. Senkan, Proc. Combust. Inst. 27 (1998) 1631–1637.
[24] M.J. Castaldi, A.M. Vincitore, S.M. Senkan, Combust. Sci. Technol. 107 (1995) 1–19.
[25] A. Turbiez, A. El Bakali, J.F. Pauwels, A. Rida, P. Meunier, Fuel 83 (2004) 933–941.
[26] N.M. Marinov, W.J. Pitz, C.K. Westbrook, M.J. Castaldi, S.M. Senkan, Combust. Sci. Technol. 116–117 (1996) 211–287.
[27] N.M. Marinov, W.J. Pitz, C.K. Westbrook, A.E. Lutz, A.M. Vincitore, S.M. Senkan, Proc. Combust. Inst. 27 (1998) 605–613.
[28] A.M. Vincitore, S.M. Senkan, Combust. Sci. Technol. 130 (1997) 233–246.
[29] J.F. Roesler, S. Martinot, C.S. McEnally, L.D. Pfefferle, J.L. Delfau, C. Vovelle, Combust. Flame 134 (2003) 249–260.
[30] C.S. McEnally, L.D. Pfefferle, A.M. Schaffer, M.B. Long, R.K. Mohammed, M.D. Smooke, M.B. Colket, Proc. Combust. Inst. 28 (2000) 2063–2070.
[31] H. Anderson, C.S. McEnally, L.D. Pfefferle, Proc. Combust. Inst. 28 (2000) 2577–2583.
[32] K.J. Hughes, T. Turanyi, A.R. Clague, M.J. Pilling, Int. J. Chem. Kinet. 33 (2001) 513–538.
[33] E. Ranzi, A. Sogaro, P. Gaffuri, G. Pennati, T. Faravelli, Combust. Sci. Technol. 96 (1994) 279–325. http://creckmodeling.chem.polimi.it/index.php/kinetic-schemes.
[34] G.P. Smith, D.M. Golden, M. Frenklach, N.W. Moriarty, B. Eiteneer, M. Goldenberg, C.T. Bowman, R.K. Hanson, S. Song, W.C. Gardiner Jr., V.V. Lissianski, Z. Qin, <http://www.me.berkeley.edu/gri_mech/>.
[35] H. Wang, X. You, A.V. Joshi, S.G. Davis, A. Laskin, F. Egolfopoulos, C.K. Law, USC Mech Version II. High-temperature combustion reaction model of H2/CO/C1–C4 Compounds. <http://ignis.usc.edu/USC_Mech_II.htm, May 2007>.
[36] W.K. Metcalfe, S.M. Burke, S.S. Ahmed, H.J. Curran, Int. J. Chem. Kinet. 45 (2013) 638–675.
[37] A. D'Anna, J.H. Kent, Combust. Flame 132 (2003) 715–722.
[38] H. Wang, M. Frenklach, Combust. Flame 96 (1994) 163–170.
[39] H. Wang, M. Frenklach, Combust. Flame 110 (1997) 173–221.
[40] N.A. Slavinskaya, P. Frank, Combust. Flame 156 (2009) 1705–1722.
[41] V. Chernov, M.J. Thomson, S.B. Dworkin, N.A. Slavinskaya, U. Riedel, Combust. Flame 161 (2014) 592–601.
[42] S.B. Dworkin, Q. Zhang, M.J. Thomson, N.A. Slavinskaya, U. Riedel, Combust. Flame 158 (2011) 1682–1695.
[43] M. Derudi, D. Polino, C. Cavallotti, Phys. Chem. Chem. Phys. 13 (2011) 21308–21318.
[44] A. Matsugi, A. Miyoshi, Int. J. Chem. Kinet. 44 (2012) 206–218.
[45] M.R. Djokic, K.M. Van Geem, C. Cavallotti, A. Frassoldati, E. Ranzi, G.B. Marin, Combust. Flame (2014) (in proof).
[46] C. Cavallotti, D. Polino, Proc. Combust. Inst. 34 (2013) 557–564.
[47] A. Cuoci, A. Frassoldati, T. Faravelli, E. Ranzi, Combust. Flame 160 (2013) 870–886.
[48] A. Cuoci, A. Frassoldati, T. Faravelli, H. Jin, Y. Wang, K. Zhang, P. Glarborg, F. Qi, Proc. Combust. Inst. 34 (2013) 1811–1818.
[49] C. Saggese, A. Frassoldati, A. Cuoci, T. Faravelli, E. Ranzi, Combust. Flame 160 (2013) 1168–1190.
[50] J.Z. Yang, L. Zhao, J.H. Cai, F. Qi, Y.Y. Li, Chin. J. Chem. Phys. 26 (2013) 245–251.
[51] A.W. Jasper, N. Hansen, Proc. Combust. Inst. 34 (2013) 279–287.
[52] G. Vourliotakis, G. Skevis, M.A. Founti, Energy Fuels 25 (2011) 1950–1963.
[53] Y. Li, J. Cai, L. Zhang, T. Yuan, K. Zhang, F. Qi, Proc. Combust. Inst. 33 (2011) 593–600.
[54] A. Matsugi, A. Miyoshi, Proc. Combust. Inst. 34 (2013) 269–277.
[55] W.K. Metcalfe, S. Dooley, F.L. Dryer, Energy Fuels 25 (2011) 4915–4936.
[56] Y.Y. Li, L.D. Zhang, Z.D. Wang, L.L. Ye, J.H. Cai, Z.J. Cheng, F. Qi, Proc. Combust. Inst. 34 (2013) 1739–1848.
[57] Y. Wang, A. Raj, S.H. Chung, Combust. Flame 160 (2013) 1667–1676.
[58] D. Parker, F. Zhang, Y.S. Kim, R.I. Kaiser, A. Landera, V. Kislov, A.M. Mebel, A. Tielens, Proc. Natl. Acad. Sci. 109 (2012) 53–58.
[59] R.I. Kaiser, D.S.N. Parker, F. Zhang, A. Landera, V.V. Kislov, A.M. Mebel, J. Phys. Chem. A 116 (2012) 4248–4258.
[60] J. Lim, J. Gore, R. Viskanta, Combust. Flame 121 (2000) 262–274.
[61] H.F. Jin, Y.Z. Wang, K.W. Zhang, H.S. Guo, F. Qi, Proc. Combust. Inst. 34 (2013) 779–786.
[62] Photonionization Cross Section Database (Version 1.0), National Synchrotron Radiation Laboratory, Hefei, China, 2011. <http://www.flame.nsrl.ustc.edu.cn/en/database.htm>.
[63] J.H. Kent, Combust. Flame 14 (1970) 279–281.
[64] Y. Li, J. Cai, L. Zhang, J. Yang, Z. Wang, F. Qi, Proc. Combust. Inst. 33 (2011) 617–624.
[65] H. Jin, W. Yuan, Y. Wang, Y. Li, F. Qi, A. Cuoci, A. Frassoldati, T. Faravelli, Proc. Combust. Inst. (2014), in press.
[66] L. Zhang, J. Cai, T. Zhang, F. Qi, Combust. Flame 157 (2010) 1686–1697.
[67] C. Cavallotti, D. Polino, A. Frassoldati, E. Ranzi, J. Phys. Chem. A 116 (2012) 3313–3324.
[68] H. Richter, J.B. Howard, Phys. Chem. Chem. Phys. 4 (2002) 2038–2055.
[69] G. Blanquart, P. Pepiot-Desjardins, H. Pitsch, Combust. Flame 156 (2009) 588–607.
[70] N.A. Slavinskaya, U. Riedel, S.B. Dworkin, M.J. Thomson, Combust. Flame 159 (2012) 979–995.
[71] C.T. Bowman, R.K. Hanson, D.F. Davidson, W.C. Gardiner Jr., V. Lissianski, G.P. Smith, D.M. Golden, M. Frenklach, M. Goldenberg. <http://www.me.berkeley.edu/gri_mech/>.
[72] S.J. Klippenstein, Y. Georgievskii, L.B. Harding, Proc. Combust. Inst. 29 (2002) 1229–1236.
[73] D.L. Baulch, C.T. Bowman, C.J. Cobos, R.A. Cox, T. Just, J.A. Kerr, M.J. Pilling, D. Stocker, J. Troe, W. Tsang, R.W. Walker, J. Warnatz, J. Phys. Chem. Ref. Data 34 (2005) 757–1397.
[74] N.K. Srinivasan, M.C. Su, J.W. Sutherland, J.V. Michael, J. Phys. Chem. A 109 (2005) 1857–1863.
[75] L.B. Harding, S.J. Klippenstein, Y. Georgievskii, Proc. Combust. Inst. 30 (2005) 985–993.
[76] A.W. Jasper, S.J. Klippenstein, L.B. Harding, B. Ruscic, J. Phys. Chem. A 111 (2007) 3932–3950.
[77] S.M. Sarathy, S. Vranckx, K. Yasunaga, M. Mehl, P. Oßwald, W.K. Metcalfe, C.K. Westbrook, W.J. Pitz, K. Kohse-Höinghaus, R.X. Fernandes, H.J. Curran, Combust. Flame 159 (2012) 2028–2055.
[78] N.K. Srinivasan, M.C. Su, J.W. Sutherland, J.V. Michael, J. Phys. Chem. A 109 (2005) 7902–7914.
[79] B. Wang, H. Hou, L.M. Yoder, J.T. Muckerman, C. Fockenberg, J. Phys. Chem. A 107 (2003) 11414–11426.
[80] S.J. Klippenstein, Y. Georgievskii, L.B. Harding, Phys. Chem. Chem. Phys. 8 (2006) 1133–1147.
[81] J.H. Kiefer, S. Santhanam, N.K. Srinivasan, R.S. Tranter, S.J. Klippenstein, M.A. Oehlschlaeger, Proc. Combust. Inst. 30 (2005) 1129–1135.
[82] M.A. Oehlschlaeger, D.F. Davidson, R.K. Hanson, Proc. Combust. Inst. 30 (2005) 1119–1127.
[83] D.L. Baulch, C.J. Cobos, R.A. Cox, C. Esser, P. Frank, T. Just, J.A. Kerr, M.J. Pilling, J. Troe, R.W. Walker, J. Warnatz, J. Phys. Chem. Ref. Data 21 (1992) 411–734.
[84] C.M. Vagelopoulos, F.N. Egolfopoulos, in: Symposium (International) on Combustion, vol. 27, 1998, pp. 513–519.
[85] X.J. Gu, M.Z. Haq, M. Lawes, R. Woolley, Combust. Flame 121 (2000) 41–58.
[86] G. Rozenchan, D.L. Zhu, C.K. Law, S.D. Tse, Proc. Combust. Inst. 29 (2002) 1461–1470.
[87] O. Park, P.S. Veloo, N. Liu, F.N. Egolfopoulos, Proc. Combust. Inst. 33 (2011) 887–894.
[88] F. Halter, T. Tahtouh, C. Mounaïm-Rousselle, Combust. Flame 157 (2010) 1825–1832.
[89] M.I. Hassan, K.T. Aung, G.M. Faeth, Combust. Flame 115 (1998) 539–550.
[90] K.J. Bosschaart, L.P.H. de Goey, Combust. Flame 136 (2004) 261–269.
[91] C. Bahrini, O. Herbinet, P.-A. Glaude, C. Schoemaecker, C. Fittschen, F. Battin-Leclerc, Chem. Phys. Lett. 534 (2012) 1–7.
[92] J.A. Miller, S.J. Klippenstein, Phys. Chem. Chem. Phys. 6 (2004) 1192–1202.
[93] W. Tsang, R.F. Hampson, J. Phys. Chem. Ref. Data 15 (1986) 1087–1279.
[94] J.T. Herron, J. Phys. Chem. Ref. Data 17 (1988) 967–1026.
[95] W. Tsang, J. Phys. Chem. Ref. Data 17 (1988) 887–951.
[96] E.W. Diau, M.C. Lin, C.F. Melius, J. Chem. Phys. 101 (1994) 3923–3927.
[97] S.G. Davis, C.K. Law, H. Wang, J. Phys. Chem. A 103 (1999) 5889–5899.
[98] Y. Georgievskii, J.A. Miller, S.J. Klippenstein, Phys. Chem. Chem. Phys. 9 (2007) 4259–4268.
[99] J.A. Miller, S.J. Klippenstein, J. Phys. Chem. A 107 (2003) 7783–7799.
[100] B.R. Giri, H. Hippler, M. Olzmann, A.N. Unterreiner, Phys. Chem. Chem. Phys. 5 (2003) 4641–4646.
[101] S. Scherer, T. Just, P. Frank, Proc. Combust. Inst. 28 (2000) 1511–1518.
[102] E.V. Shafir, I.R. Slagle, V.D. Knyazev, J. Phys. Chem. A 107 (2003) 8893–8903.
[103] A. Burcat, M. Dvinyaninov, Int. J. Chem. Kinet. 29 (1997) 505–514.
[104] C.L. Rasmussen, M.S. Skjøth-Rasmussen, A.D. Jensen, P. Glarborg, Proc. Combust. Inst. 30 (2005) 1023–1031.
[105] N. Hansen, J.A. Miller, P.R. Westmoreland, T. Kasper, K. Kohse-Höinghaus, J. Wang, T.A. Cool, Combust. Flame 156 (2009) 2153–2164.
[106] J.A. Miller, C.F. Melius, Amer. Chem. Soc. 202 (1991) 1155.
[107] A. Laskin, H. Wang, C.K. Law, Int. J. Chem. Kinet. 32 (2000) 589–614.
[108] C.A. Taatjes, S.J. Klippenstein, N. Hansen, J.A. Miller, T.A. Cool, J. Wang, M.E. Law, P.R. Westmoreland, Phys. Chem. Chem. Phys. 7 (2005) 806–813.
[109] S.J. Klippenstein, L.B. Harding, Y. Georgievskii, Proc. Combust. Inst. 31 (2007) 221–229.
[110] R. Sivaramakrishnan, J.V. Michael, Proc. Combust. Inst. 33 (2011) 225–232.
[111] M.A. Oehlschlaeger, D.F. Davidson, R.K. Hanson, Proc. Combust. Inst. 31 (2007) 211–219.
[112] T. Seta, M. Nakajima, A. Miyoshi, J. Phys. Chem. A 110 (2006) 5081–5090.
[113] K. Narayanaswamy, G. Blanquart, H. Pitsch, Combust. Flame 157 (2010) 1879–1898.
[114] V.V. Kislov, A.M. Mebel, J. Phys. Chem. A 111 (2007) 3922–3931.
[115] V.V. Kislov, N.I. Islamova, A.M. Kolker, S.H. Lin, A.M. Mebel, J. Chem. Theory Comput. 1 (2005) 908–924.
[116] L. Vereecken, H.F. Bettinger, J. Peeters, Phys. Chem. Chem. Phys. 4 (2002) 2019–2027.
[117] L. Vereecken, J. Peeters, Phys. Chem. Chem. Phys. 5 (2003) 2807–2817.
[118] H. Richter, J.B. Howard, Prog. Energy Combust. Sci. 26 (2000) 565–608.

[119] A. Cuoci, A. Frassoldati, T. Faravelli, E. Ranzi, Combust. Flame 156 (2009) 2010–2022.
[120] A. Cuoci, A. Frassoldati, T. Faravelli, E. Ranzi, Energy Fuels 27 (2013) 7730–7753.
[121] H.F. Jin, A. Cuoci, A. Frassoldati, T. Faravelli, Y.Z. Wang, Y.Y. Li, F. Qi, Combust. Flame 161 (2014) 657–670.
[122] E. Goos, A. Burcat, B. Ruscic, Ideal Gas Thermochemical Database with Updates from Active Thermochemical Table, 2005, <ftp://ftp.technion.ac.il/pub/supported/aetdd/thermodunamics>.
[123] R.J. Kee, J. Warnatz, J.A. Miller, Chemkin II: A Fortran Chemical Kinetics Package for the Evaluation of Gas-phase Viscosities, Conductivities and Diffusion Coefficient, Sandia National Laboratory, 1983.
[124] S. Chapman, T.G. Cowling, The Mathematical Theory of Non-Uniform Gases, Cambridge University Press, Cambridge, 1970.
[125] R.J. Hall, J. Quant. Spectrosc. Radiat. Transfer 49 (1993) 517–523.
[126] F. Qi, Proc. Combust. Inst. 34 (2013) 33–63.
[127] P.R. Westmoreland, A.M. Dean, J.B. Howard, J.P. Longwell, J. Phys. Chem. 93 (1989) 8171–8180.
[128] R.D. Kern, K. Xie, Prog. Energy Combust. Sci. 17 (1991) 191–210.
[129] J. Appel, H. Bockhorn, M. Frenklach, Combust. Flame 121 (2000) 122–136.
[130] C.F. Melius, M.E. Colvin, N.M. Marinov, W.J. Pitz, S.M. Senkan, Proc. Combust. Inst. 26 (1996) 685–692.
[131] L.V. Moskaleva, A.M. Mebel, M.C. Lin, Proc. Combust. Inst. 26 (1996) 521–526.
[132] S.K. Gulati, R.W. Walker, J. Chem. Soc., Faraday Trans. 85 (1989) 1799–1812.
[133] H.R. Zhang, E.G. Eddings, A.F. Sarofim, C.K. Westbrook, Proc. Combust. Inst. 32 (2009) 377–385.
[134] B. Shukla, M. Koshi, Combust. Flame 158 (2011) 369–375.
[135] B. Shukla, M. Koshi, Combust. Flame 159 (2012) 3589–3596.
[136] A.W. Jasper, S.J. Klippenstein, L.B. Harding, Proc. Combust. Inst. 32 (2009) 279–286.
[137] J.D. DeSain, S.J. Klippenstein, J.A. Miller, C.A. Taatjes, J. Phys. Chem. A 107 (2003) 4415–4427.
[138] W. Tsang, J. Phys. Chem. Ref. Data 20 (1991) 221–273.
[139] D.L. Baulch, C.J. Cobos, R.A. Cox, P. Frank, G. Hayman, T. Just, J.A. Kerr, T. Murrells, M.J. Pilling, J. Troe, R.W. Walker, J. Warnatz, J. Phys. Chem. Ref. Data 23 (1994) 847–848.